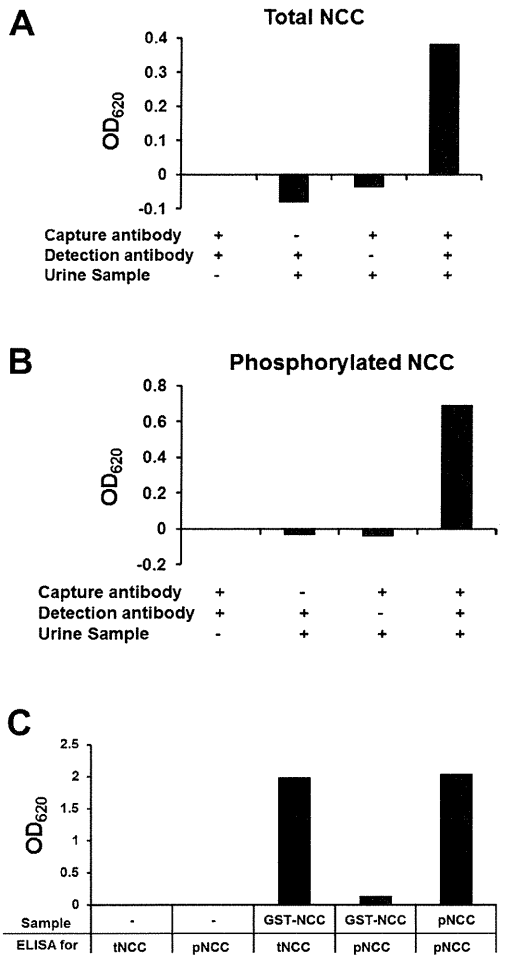

Fig. 2. Confirmation of specificity of the sandwich ELISAs. *A* and *B*: validation of sandwich ELISAs for tNCC and pNCC. Without the capture and detection antibodies, the signals for tNCC (*A*) and pNCC (*B*) were not detected. *C*: phosphospecificity of sandwich ELISA for pNCC. GST-NCC and pNCC peptide were used as standards for sandwich ELISA for tNCC and pNCC, respectively. GST-NCC was not phosphorylated. Our sandwich ELISA for pNCC did not detect GST-NCC but did detect the pNCC peptide.

able rabbit anti-NCC (Millipore; Ref. 20). In the present study, we generated another guinea pig anti-NCC antibody by immunizing animals with keyhole limpet hemocyanin-conjugated synthetic peptide corresponding to residues 1–16 of NCC (MAELPTTETPGDATLC). The serum was affinity purified with the antigen peptides. The specificities of the antibodies were verified by antigen absorption tests (data not shown). Alkaline phosphatase-conjugated anti-IgG antibodies and Western Blue substrate (Promega, Madison, WI) were used for immunoblotting. Scanned images of the NCC bands at ~150 kDa were quantified by using ImageJ software (National Institutes of Health, Bethesda, MD).

Sandwich ELISA. Rabbit anti-tNCC (75–90) (0.18 μg/well) and anti-pT55NCC (0.9 μg/well) antibodies in 100 μl of bicarbonate buffer (15 mM Na_2CO_3, 35 mM $NaHCO_3$) were applied to 96-well ELISA plates (IWAKI, Tokyo, Japan) and incubated at 4°C for 96 h for immobilization. The anti-NCC antibodies used in the assays share no antigenic homology with other proteins including homologous NKCC1 and NKCC2. After being washed with 200 μl of wash buffer (TBS-0.02% Tween20) three times and being blocked with 200 μl of 1.5% (wt/vol) albumin in TBS-0.02% Tween20 for 30 min at room temperature, 100 μl of urinary exosome samples or standard proteins for tNCC and pNCC were applied to the wells. After a 2-h incubation at 37°C under gentle shaking, the plates were washed six times with a wash buffer (TBS-0.02% Tween20). Then, 100 μl of guinea pig anti-tNCC antibody (1–16; 0.16 μg/well) and anti-tNCC antibody (75–90; 0.38 μg/well) in EIA buffer (TBS-0.02% Tween20 and 0.2% BSA) were applied to each well for the tNCC and pNCC assays, respectively, for 2 h at 37°C under gentle shaking. Plates were washed with wash buffer again for seven times, and 100 μl AP-labeled anti-guinea pig antibody in EIA buffer (1:2,000 dilution) were added as a secondary antibody and incubated for 1 h at 37°C. After being washed eight times, 100 μl of BluePhos (KPL, Gaithersburg, MD) were applied and incubated for 10 min. The signals at 620 nm were obtained by a plate reader (Spectrafluor; Tecan Japan, Kanagawa, Japan). All of the antibodies used in this study are available in small amounts upon request.

Patients. Between July 2012 and March 2013, we recruited 93 patients who were treated as chronic kidney disease patients in the nephrology department of Tokyo Medical and Dental University. The Medical Research Ethics Committee of Tokyo Medical and Dental University approved this study (Approval No. 1031).

Clinical data collection. Medical records were used to collect data on age, sex, blood pressure (BP), serum albumin, sodium, potassium, creatinine (Cr), chloride, and urine Cr, urine protein, and urine sodium. Estimated glomerular filtration rates (eGFRs) were calculated with the following previously published Japanese eGFR equation (13): eGFR [ml·min·1.73 m^{-2}] = 0.741 × 175 × $(age)^{-0.287}$ × $(serum\ Cr)^{-1.094}$ × 0.739 (if female).

We used the following formula to calculate fractional excretion of sodium (FE_{Na}): FE_{Na} [%] = [serum Cr × urinary sodium/serum sodium × urinary Cr] × 100.

Statistical methods. Data are expressed as means ± SD. Comparisons between the two groups were performed with unpaired *t*-tests. The relationship of urinary tNCC and pNCC with continuous variables was examined by Pearson's correlation coefficient. The multivariable regression analysis was created based on the variables that had a simple correlation of $P < 0.05$ to eGFR and FE_{Na}.

RESULTS AND DISCUSSION

Development of sandwich ELISA for tNCC and pNCC. We needed to modify an ultracentrifugation method of urine exosome preparation for our sandwich ELISA since the original

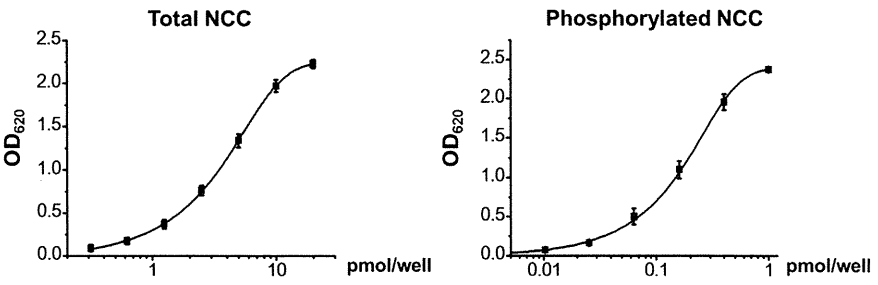

Fig. 3. Sensitivity of sandwich ELISA for tNCC and pNCC. The sandwich ELISA for tNCC and pNCC detected as little as 3 pmol/ml and 100 fmol/ml of standard proteins, respectively. OD_{260}, optical density at 260.

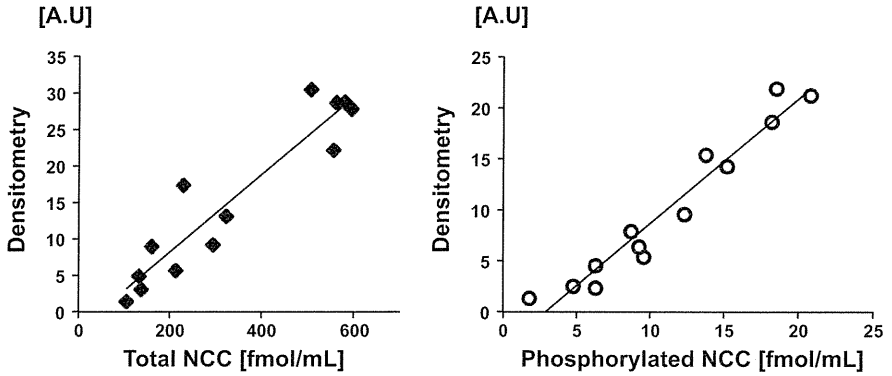

Fig. 4. Correlation between sandwich ELISA and immunoblot. Urine samples were collected from 13 healthy volunteers. After preparation of exosomes, the samples were divided into sandwich ELISA samples and immunoblot samples. The amount of tNCC and pNCC measured by the sandwich ELISA was highly correlated with the band intensities obtained by immunoblots. ($r = 0.94$, $r = 0.97$, respectively). A.U, arbitrary unit.

ultracentrifugation method (23) results in the formation of tight pellets that cannot be dissolved in a buffered solution for ELISA. Tamm-Horsfall protein (THP), also known as uromodulin, is the most abundant protein in human urine (22), and it is known to form polymeric meshwork (31). Accordingly, we speculated that the THP polymers could make the pellet insoluble, and we incorporated a DTT treatment step into the original ultracentrifugation method to disrupt the networks, as described previously (7, 23). We also modified the centrifugation speed and optimized the buffer and the detergent for exosome preparation for our ELISA assays. As for the detergent, we judged that 0.02% Tween20 was enough to demolish the exosomes and to extract NCC since we did not observe any significant changes of signals in our ELISA if the concentrations of Tween20 was increased up to 0.1% or a more potent detergent, 0.1% TritonX-100, was used instead of Tween20.

This modified procedure allowed us to detect a pNCC signal (Fig. 1*A*). We determined reproducibility of this exosome preparation by analyzing a single urine sample in six different tubes. NCC and other exosome-associated proteins (THP, TSG101, and AQP2) were reproducibly detected by immunoblots. The average coefficient of variation was <10%.

The principle of our sandwich ELISA is summarized in Fig. 1*B*. As shown in Fig. 2, *A* and *B*, the elimination of either the capture or detection antibody in the assays resulted in no signal detection, confirming that there were no nonspecific signals in these assays. Then, we tested the phosphospecificity of sandwich ELISA for pNCC. Although we previously demonstrated the phosphospecificity of the antibody to detect p55T in NCC protein (3), we also verified it in our sandwich ELISA. As shown in Fig. 2*C*, while the pNCC peptide was detected by ELISA for pNCC, GST-NCC, which was not phosphorylated (confirmed by immunoblot with anti-p55T antibody, data not shown), was not detected. This result indicated that the sandwich ELISA for pNCC maintained high phosphospecificity.

We further evaluated the sensitivities of these sandwich ELISA systems. The sandwich ELISAs for tNCC and pNCC detected as little as 3 pmol/ml and 100 fmol/ml of each standard, respectively (Fig. 3). Since the active form of NCC is the phosphorylated form, pNCC in urine may be a better parameter than tNCC to estimate the activity of NCC in the kidney. In this respect, it was fortunate for us that the ELISA for pNCC showed a higher sensitivity than the tNCC ELISA,

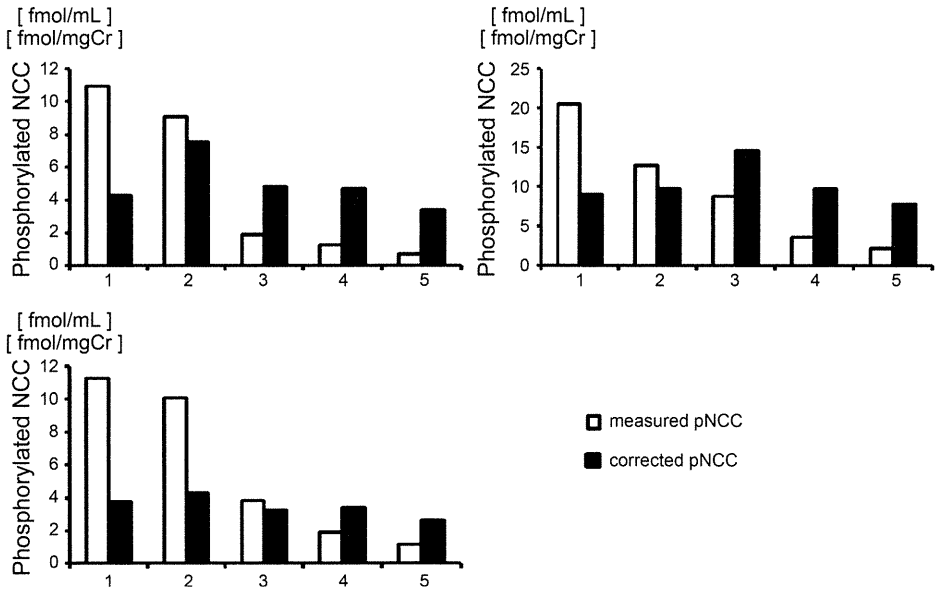

Fig. 5. Urinary NCC can be corrected by urinary creatinine (Cr). We measured pNCC in 5 different spot urine samples collected within a day from 3 different subjects. pNCC concentration corrected by Cr was constant among the 5 spot urine samples.

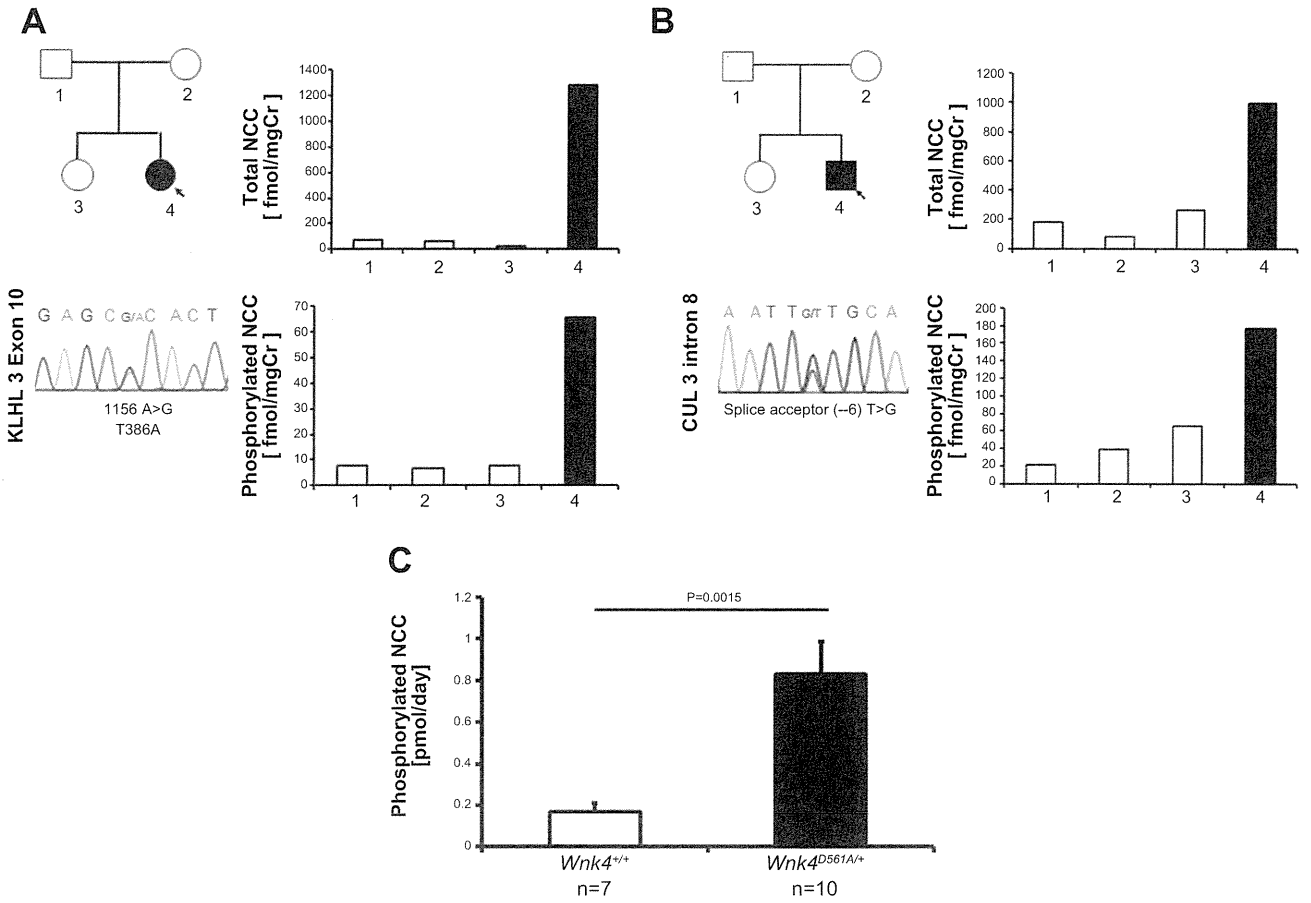

Fig. 6. Excretion of NCC in urine exosomes in pseudohypoaldosteronism type II (PHAII) family members and PHAII model mice. *A* and *B*: closed symbol/bar indicates the family members carrying the PHAII mutation. The patients in *family A* and *B* have the T386A KLHL3 mutation and CUL3 mutation [splice acceptor (−6) T > G], respectively. Spot urine samples were collected from all members of the 2 families. Excretion of tNCC and pNCC in urine exosomes was increased only in the family members carrying the mutations. (*C*). Excretion of pNCC in urine exosomes was increased in PHAII model mice ($Wnk4^{D561A/+}$ knockin mice). Closed symbol/bar indicates PHAII model mice. Urine samples were collected for 24 h.

which might be due to the high sensitivity of anti-p-T55 antibody used for capturing pNCC.

Correlation between immunoblots and sandwich ELISA. We examined the correlation between sandwich ELISA and NCC immunoblot, which has been used to compare the relative abundance of urinary NCC proteins (12, 14, 27). Spot urine samples were collected from 13 healthy volunteers. After the preparation of exosomes, the samples were divided into sandwich ELISA and immunoblot samples. The immunoblot signals of tNCC and pNCC (~150 kDa) were obtained by the capture antibodies that were used in ELISA and were analyzed by densitometry. The amounts of tNCC and pNCC measured by the sandwich ELISAs were highly correlated with the immunoblot data (r = 0.94, r = 0.97, respectively; Fig. 4), validating that the ELISA assays could measure the amounts of full-length NCC and pNCC although the epitopes of capture and detection antibodies were relatively closely located. The very close correlation of pNCC ELISA and its immunoblot data also verified the phosphospecificity of pNCC ELISA in urine samples.

Urinary exosomal NCC can be normalized with urinary Cr. To evaluate the amount of urinary tNCC and pNCC in spot urine samples, we investigated a method to correct the amount of tNCC and pNCC in spot urine samples from a single subject. Normalization of urinary biomarkers is an unresolved issue. Fernández-Llama (7) previously reported that exosomal proteins can be normalized by THP. Likewise, urinary exosome markers, such as TSG101, Alix, or Hsp70 (7, 23, 33), may be used for the normalization of urinary exosomal proteins. However, it is unknown if these proteins are constant under various

Table 1. *Urinary excretion of total and phosphorylated NCC in Gitelman's syndrome*

	1	2	3	4
Mutation found in NCC gene	L849H (hetero)	V578M (hetero) delTT[1] (hetero)	V578M (hetero) delTT[1] (hetero)	T180K (homo)
Total NCC, fmol/mg Cr	ND	ND	ND	ND
Phosphorylated NCC, fmol/mg Cr	0.30	ND	2.51	ND

NCC, Na-Cl cotransporter; homo, homozygous mutation; hetero, heterozygous mutation; Cr, creatinine; ND, not detected. [1]2-bp (TT) deletion at 2543–2544.

Table 2. *Main characteristics of participants*

	Total NCC (n = 39)	Phosphorylated NCC (n = 61)
Age, yr	65.0 ± 14.7	63.5 ± 14.6
Male, %	25 (64)	39 (64)
Diabetes, %	8 (21)	11 (18)
Hypertension, %	29 (75)	47 (77)
eGFR, ml·min·1.73 m^{-2}	49.7 ± 17.9	50.3 ± 18.1
Systolic BP, mmHg	124.9 ± 16.0	126.3 ± 17.7
Diastolic BP, mmHg	75.4 ± 11.3	76.0 ± 11.9
Serum albumin, mg/dl	4.3 ± 0.3	4.3 ± 0.3
Serum sodium, mEq/l	140.8 ± 2.0	140.3 ± 1.9
Serum potassium, mEq/l	4.4 ± 0.3	4.4 ± 0.4
Serum chloride, mEq/l	106.0 ± 2.6	106.0 ± 2.7

Values are means ± SE. eGFR, estimated glomerular filtration rate; BP, blood pressure.

pathophysiological conditions, and their quantitative measurements are still not easy for a large number of clinical samples. Although normalization of urinary biomarkers to urine Cr has been recognized to be misleading especially when GFR is changing (28), most clinical urine sample measurements are usually corrected by urine Cr. Zhou et al. (33) reported that specific exosome-associated proteins normalized by Cr are almost equal within samples from the same person, and they also discussed that normalization by urine Cr is currently the best option for clinical study since nornmalization of urine flow rate is theoretically the best but rarely practical. Therefore, we tested urinary Cr for normalization in our assays. We measured pNCC in five different spot urine samples within a day from three different subjects. The pNCC concentrations corrected by the Cr level were almost equal among the five spot urine samples (Fig. 5) from the same subject. This result suggests that a single spot urine sample can be used to estimate the total excretion of pNCC for 24 h.

Measurements of tNCC and pNCC in patients with PHAII and Gitelman's syndrome. To evaluate whether the activity of NCC in the kidney would reflect the excretion of tNCC and pNCC in urinary exosomes, we first collected urine samples from two PHAII families and measured the excretion of tNCC and pNCC in urinary exosomes since NCC is constitutively activated in PHAII. Very recently, we reported that WNK4 is a target of Cullin3-KLHL3 E3 ligase and that the impaired ubiquitination and subsequently increased level of WNK4 in the kidney could activate downstream OSR1/SPAK-NCC signaling, which is the major common pathogenesis of PHAII by mutations in three different genes (29). In *family A*, the patient carried a novel de novo mutation in the KLHL3 gene

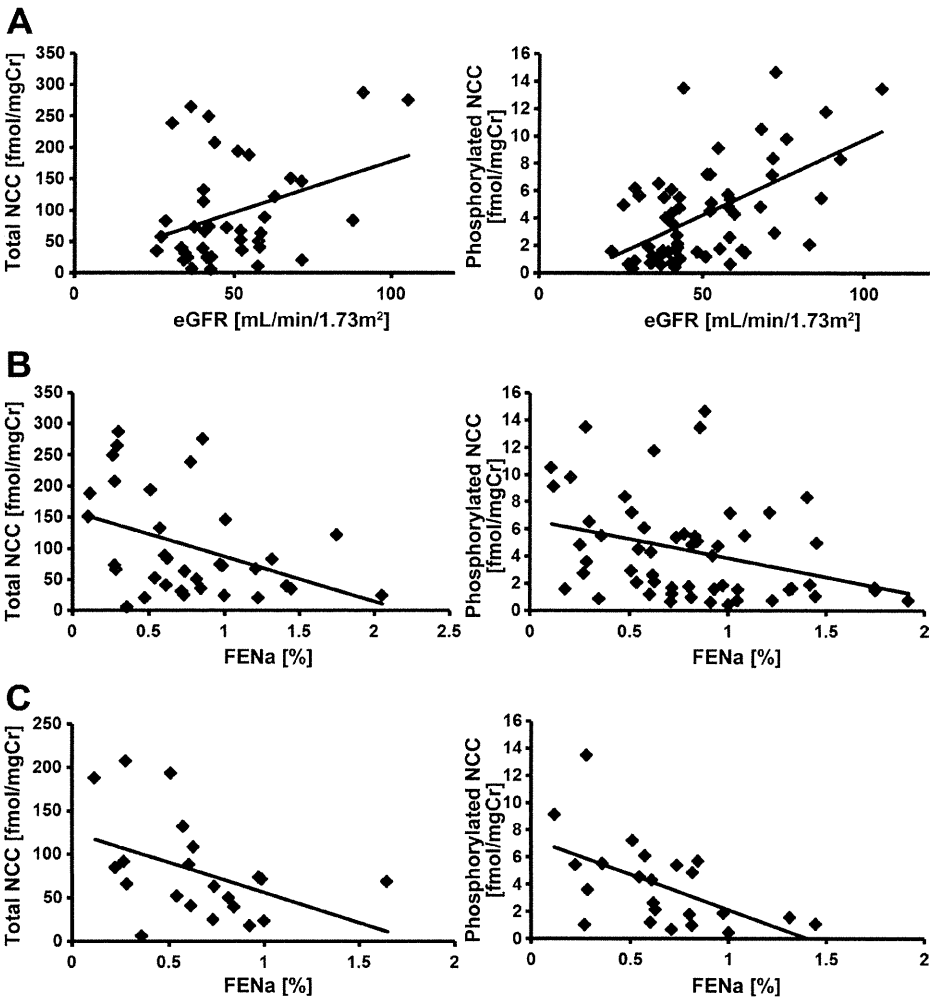

Fig. 7. Correlation of tNCC or pNCC with estimated glomerular filtration rates (eGFR; *A*) and fractional excretion of sodium (FE_{Na}; *B* and *C*). These scatterplots show that these 2 parameters were significantly correlated with total and pNCC. Data in *C* are from the patients whose eGFR were in the range from 40 to 60 ml·min·1.73 m^{-2}.

(heterozygous T386A; Fig. 6*A*). Since this mutation is located within the hot spot of PHAII mutations in the kelch domain (1), and there was genotype-phenotype correlation within the family, we regarded this mutation as a PHAII-causing mutation (a case report is in preparation). In *family B*, a heterozygous novel de novo mutation in intron 8 of the CUL3 gene [splice acceptor (−6) T > G] was identified in the patient (Fig. 6*B*). The skipping of exon 9, postulated as a consequence of the CUL3 gene mutations (1), was confirmed in the patient's white blood cells by RT-PCR (21). As shown in Fig. 6, *A* and *B*, the excretion of tNCC and pNCC in urinary exosomes was robustly increased in the family members who carried each mutation in the two families.

We also confirmed this finding in our PHAII model mice (*Wnk4*$^{D561A/+}$ knockin mice) in which NCC is constitutively phosphorylated and activated. We only measured urinary pNCC in the PHAII model mice since the guinea pig antibody used in the sandwich ELISA for tNCC only recognizes human NCC. As shown in Fig. 6*C*, the level of pNCC was highly increased in the urine of the PHAII model mice.

Furthermore, we corrected urine samples from four Gitelman syndrome patients (16) and measured the excretion of tNCC and pNCC (Table 1). The loss-of-function of NCC is the cause of Gitelman's syndrome (25), and there was already preliminary data that the urinary excretion of NCC was significantly reduced (12). In all of the patients that we tested, the level of tNCC was under the detection limit, and pNCC levels were under the detection limit in two patients and low in the other two patients (0.30 and 2.51 fmol/mg Cr, respectively) compared with the mean values in outpatients with eGFR > 60 ml·min·1.73 m^{-2} (8.1 ± 5.4 fmol/mg Cr; n = 13).

These data in PHAII and Gitelman's syndrome patients indicate that urinary excretion of tNCC and pNCC reflects NCC activity in the kidney and that our ELISA assays are detecting NCC specifically. Phosphorylation of NCC in the kidney is now widely recognized as an excellent marker to reflect the in vivo activity of NCC (8). However, it is poorly understood at present how the pNCC localized to the apical plasma membranes of the distal tubules is excreted in urine, especially into the exosomes. Nonetheless, previous studies (12, 17, 27) and the present study clearly suggest that tNCC and pNCC in the urine may reflect the amounts in the kidney.

Analysis of tNCC and pNCC in urinary exosomes in outpatients. Since the initial purpose of developing ELISA assays for urinary NCC was to establish assays to predict thiazide sensitivity as well as to help to diagnose PHAII and Gitelman's syndrome, we sought to gather more data on urinary NCC excretion not only in the specific genetic diseases but also in a more general population of patients with different clinical backgrounds. We measured urinary tNCC and pNCC in 93 outpatients from the Nephrology Department of Tokyo Medical and Dental University. Most of these outpatients had chronic kidney diseases. The 32 patients with proteinuria were excluded since urinary protein levels >30 mg/dl interfered with our ELISA. We measured urinary tNCC and pNCC in 61 patients. We could detect urinary pNCC in all 61 patients, but the measurement of tNCC was successful in only 39 patients, probably due to the lower sensitivity of the tNCC assay. Patient characteristics are shown in Table 2. The participants were predominantly male (64% in both groups) with a mean (±SD) age of 65.0 ± 14.7 yr in the tNCC group and 63.5 ± 14.6 yr in the pNCC group. The overall mean eeGFR was 49.7 ± 17.9 ml·min·1.73 m^{-2} in the tNCC group and 50.3 ± 18.1 ml·min·1.73 m^{-2} in pNCC group. Eight (21%) and eleven (18%) patients in the tNCC and pNCC groups had diabetes mellitus, respectively. Twenty-nine (75%) patients in the tNCC group and forty-seven (77%) patients in the pNCC group had hypertension.

We found interesting correlations between the clinical data and the excretion of NCC in urinary exosomes (Fig. 7). We found that excretion of tNCC and pNCC in urinary exosomes was positively correlated with eGFR (r = 0.36, P < 0.05; r = 0.56, P < 0.0001, respectively; Fig. 7*A*). This decrease of tNCC and pNCC excretion may come from the decreased number of nephrons. Thus analyses of nephron segment-specific proteins in urine exosomes would be new tools to evaluate kidney function from viewpoints other than GFR. We also found that the excretion of tNCC and pNCC in urinary exosomes negatively correlates with the FE_{Na} (r = −0.47, P < 0.01, r = −0.62, P < 0.001, respectively; Fig. 7*B*). The correlation was still evident when the analysis was limited in the patients with similar eGFR (40~60 ml·min·1.73 m^{-2}; Fig. 7*C*). Further studies are necessary to elucidate the significance of these correlations. Systolic BP, diastolic BP, serum albumin, serum sodium, serum potassium, and serum chloride were not correlated with tNCC or pNCC excretion (data not shown).

In summary, we developed sandwich ELISAs for tNCC and pNCC in urinary exosomes. This assay enabled us to estimate the activity of NCC in the human kidney and may be useful not only for the diagnosis of PHAII and Gitelman syndrome but also for predicting thiazide sensitivity in hypertensive patients with normal GFR in the future.

GRANTS

This study was supported in part by Grants-in-Aid for Scientific Research (S) from the Japan Society for the Promotion of Science, Health Labor Science Research Grant from the Ministry of Health Labor and Welfare, Salt Science Research Foundation (No. 1026, 1228), and Takeda Science Foundation.

DISCLOSURES

No conflicts of interest, financial or otherwise, are declared by the author(s).

AUTHOR CONTRIBUTIONS

Author contributions: K.I. and T. Mori performed experiments; K.I. and S.U. analyzed data; K.I. prepared figures; K.I., T. Mori, T.A., H.K., S.N., N.K., F.K., T. Morimoto, M.H., E.S., T.R., S.S., and S.U. approved final version of manuscript; S.U. conception and design of research; S.U. interpreted results of experiments; S.U. drafted manuscript; S.U. edited and revised manuscript.

REFERENCES

1. **Boyden LM, Choi M, Choate KA, Nelson-Williams CJ, Farhi A, Toka HR, Tikhonova IR, Bjornson R, Mane SM, Colussi G, Lebel M, Gordon RD, Semmekrot BA, Poujol A, Välimäki MJ, De Ferrari ME, Sanjad SA, Gutkin M, Karet FE, Tucci JR, Stockigt JR, Keppler-Noreuil KM, Porter CC, Anand SK, Whiteford ML, Davis ID, Dewar SB, Bettinelli A, Fadrowski JJ, Belsha CW, Hunley TE, Nelson RD, Trachtman H, Cole TR, Pinsk M, Bockenhauer D, Shenoy M, Vaidyanathan P, Foreman JW, Rasoulpour M, Thameem F, Al-Shahrouri HZ, Radhakrishnan J, Gharavi AG, Goilav B, Lifton RP.** Mutations in kelch-like 3 and cullin 3 cause hypertension and electrolyte abnormalities. *Nature* 482: 98–102, 2012.
2. **Chiga M, Rafiqi FH, Alessi DR, Sohara E, Ohta A, Rai T, Sasaki S, Uchida S.** Phenotypes of pseudohypoaldosteronism type II caused by the WNK4 D561A missense mutation are dependent on the WNK-OSR1/SPAK kinase cascade. *J Cell Sci* 124: 1391–1395, 2011.

3. **Chiga M, Rai T, Yang SS, Ohta A, Takizawa T, Sasaki S, Uchida S.** Dietary salt regulates the phosphorylation of OSR1/SPAK kinases and the sodium chloride cotransporter through aldosterone. *Kidney Int* 74: 1403–1409, 2008.
4. **Câmpean V, Kricke J, Ellison D, Luft FC, Bachmann S.** Localization of thiazide-sensitive Na^+-Cl^- cotransport and associated gene products in mouse DCT. *Am J Physiol Renal Physiol* 281: F1028–F1035, 2001.
5. **Dimov I, Jankovic Velickovic L, Stefanovic V.** Urinary exosomes. *Scientific World Journal* 9: 1107–1118, 2009.
6. **Ellison DH, Velázquez H, Wright FS.** Thiazide-sensitive sodium chloride cotransport in early distal tubule. *Am J Physiol Renal Fluid Electrolyte Physiol* 253: F546–F554, 1987.
7. **Fernández-Llama P, Khositseth S, Gonzales PA, Star RA, Pisitkun T, Knepper MA.** Tamm-Horsfall protein and urinary exosome isolation. *Kidney Int* 77: 736–742, 2010.
8. **Gamba G.** Regulation of the renal Na^+-Cl^- cotransporter by phosphorylation and ubiquitylation. *Am J Physiol Renal Physiol* 303: F1573–F1583, 2012.
9. **Gamba G, Miyanoshita A, Lombardi M, Lytton J, Lee WS, Hediger MA, Hebert SC.** Molecular cloning, primary structure, and characterization of two members of the mammalian electroneutral sodium-(potassium)-chloride cotransporter family expressed in kidney. *J Biol Chem* 269: 17713–17722, 1994.
10. **Gonzales PA, Pisitkun T, Hoffert JD, Tchapyjnikov D, Star RA, Kleta R, Wang NS, Knepper MA.** Large-scale proteomics and phosphoproteomics of urinary exosomes. *J Am Soc Nephrol* 20: 363–379, 2009.
11. **Gordon RD.** Syndrome of hypertension and hyperkalemia with normal glomerular filtration rate. *Hypertension* 8: 93–102, 1986.
12. **Joo KW, Lee JW, Jang HR, Heo NJ, Jeon US, Oh YK, Lim CS, Na KY, Kim J, Cheong HI, Han JS.** Reduced urinary excretion of thiazide-sensitive Na-Cl cotransporter in Gitelman syndrome: preliminary data. *Am J Kidney Dis* 50: 765–773, 2007.
13. **Matsuo S, Imai E, Horio M, Yasuda Y, Tomita K, Nitta K, Yamagata K, Tomino Y, Yokoyama H, Hishida A; Collaborators developing the Japanese equation for estimated GFR.** Revised equations for estimated GFR from serum creatinine in Japan. *Am J Kidney Dis* 53: 982–992, 2009.
14. **Mayan H, Attar-Herzberg D, Shaharabany M, Holtzman EJ, Farfel Z.** Increased urinary Na-Cl cotransporter protein in familial hyperkalaemia and hypertension. *Nephrol Dial Transplant* 23: 492–496, 2008.
15. **Mischak H, Delles C, Klein J, Schanstra JP.** Urinary proteomics based on capillary electrophoresis-coupled mass spectrometry in kidney disease: discovery and validation of biomarkers, and clinical application. *Adv Chronic Kidney Dis* 17: 493–506, 2010.
16. **Monkawa T, Kurihara I, Kobayashi K, Hayashi M, Saruta T.** Novel mutations in thiazide-sensitive Na-Cl cotransporter gene of patients with Gitelman's syndrome. *J Am Soc Nephrol* 11: 65–70, 2000.
17. **Moon PG, Lee JE, You S, Kim TK, Cho JH, Kim IS, Kwon TH, Kim CD, Park SH, Hwang D, Kim YL, Baek MC.** Proteomic analysis of urinary exosomes from patients of early IgA nephropathy and thin basement membrane nephropathy. *Proteomics* 11: 2459–2475, 2011.
18. **Moon PG, You S, Lee JE, Hwang D, Baek MC.** Urinary exosomes and proteomics. *Mass Spectrom Rev* 30: 1185–1202, 2011.
19. **Mosley K, Tam FW, Edwards RJ, Crozier J, Pusey CD, Lightstone L.** Urinary proteomic profiles distinguish between active and inactive lupus nephritis. *Rheumatology (Oxford)* 45: 1497–1504, 2006.
20. **Ohno M, Uchida K, Ohashi T, Nitta K, Ohta A, Chiga M, Sasaki S, Uchida S.** Immunolocalization of WNK4 in mouse kidney. *Histochem Cell Biol* 136: 25–35, 2011.
21. **Osawa M, Ogura Y, Isobe K, Uchida S, Nonoyama S, Kawaguchi H.** CUL3 gene analysis enables early intervention for pediatric pseudohypoaldosteronism type II in infancy. *Pediatr Nephrol* 28: 1881–1884, 2013.
22. **Pisitkun T, Johnstone R, Knepper MA.** Discovery of urinary biomarkers. *Mol Cell Proteomics* 5: 1760–1771, 2006.
23. **Pisitkun T, Shen RF, Knepper MA.** Identification and proteomic profiling of exosomes in human urine. *Proc Natl Acad Sci USA* 101: 13368–13373, 2004.
24. **Rovin BH, Birmingham DJ, Nagaraja HN, Yu CY, Hebert LA.** Biomarker discovery in human SLE nephritis. *Bull NYU Hosp Jt Dis* 65: 187–193, 2007.
25. **Simon DB, Nelson-Williams C, Bia MJ, Ellison D, Karet FE, Molina AM, Vaara I, Iwata F, Cushner HM, Koolen M, Gainza FJ, Gitleman HJ, Lifton RP.** Gitelman's variant of Bartter's syndrome, inherited hypokalaemic alkalosis, is caused by mutations in the thiazide-sensitive Na-Cl cotransporter. *Nat Genet* 12: 24–30, 1996.
26. **van Balkom BW, Pisitkun T, Verhaar MC, Knepper MA.** Exosomes and the kidney: prospects for diagnosis and therapy of renal diseases. *Kidney Int* 80: 1138–1145, 2011.
27. **van der Lubbe N, Jansen PM, Salih M, Fenton RA, van den Meiracker AH, Danser AH, Zietse R, Hoorn EJ.** The phosphorylated sodium chloride cotransporter in urinary exosomes is superior to prostasin as a marker for aldosteronism. *Hypertension* 60: 741–748, 2012.
28. **Waikar SS, Sabbisetti VS, Bonventre JV.** Normalization of urinary biomarkers to creatinine during changes in glomerular filtration rate. *Kidney Int* 78: 486–494, 2010.
29. **Wakabayashi M, Mori T, Isobe K, Sohara E, Susa K, Araki Y, Chiga M, Kikuchi E, Nomura N, Mori Y, Matsuo H, Murata T, Nomura S, Asano T, Kawaguchi H, Nonoyama S, Rai T, Sasaki S, Uchida S.** Impaired KLHL3-mediated ubiquitination of WNK4 causes human hypertension. *Cell Rep* 2013.
30. **Weissinger EM, Wittke S, Kaiser T, Haller H, Bartel S, Krebs R, Golovko I, Rupprecht HD, Haubitz M, Hecker H, Mischak H, Fliser D.** Proteomic patterns established with capillary electrophoresis and mass spectrometry for diagnostic purposes. *Kidney Int* 65: 2426–2434, 2004.
31. **Wiggins RC.** Uromucoid (Tamm-Horsfall glycoprotein) forms different polymeric arrangements on a filter surface under different physicochemical conditions. *Clin Chim Acta* 162: 329–340, 1987.
32. **Yang SS, Morimoto T, Rai T, Chiga M, Sohara E, Ohno M, Uchida K, Lin SH, Moriguchi T, Shibuya H, Kondo Y, Sasaki S, Uchida S.** Molecular pathogenesis of pseudohypoaldosteronism type II: generation and analysis of a Wnk4(D561A/+) knockin mouse model. *Cell Metab* 5: 331–344, 2007.
33. **Zhou H, Yuen PS, Pisitkun T, Gonzales PA, Yasuda H, Dear JW, Gross P, Knepper MA, Star RA.** Collection, storage, preservation, and normalization of human urinary exosomes for biomarker discovery. *Kidney Int* 69: 1471–1476, 2006.

Journal of Dermatological Science 70 (2013) 26–33

Contents lists available at SciVerse ScienceDirect

Journal of Dermatological Science

journal homepage: www.elsevier.com/jds

Immunolocalization and translocation of aquaporin-5 water channel in sweat glands

Risako Inoue [a,b], Eisei Sohara [b], Tatemitsu Rai [b], Takahiro Satoh [c], Hiroo Yokozeki [a], Sei Sasaki [b], Shinichi Uchida [b,*]

[a] Department of Dermatology, Graduate School of Medical and Dental Sciences, Tokyo Medical and Dental University, Tokyo, Japan
[b] Department of Nephrology, Graduate School of Medical and Dental Sciences, Tokyo Medical and Dental University, Tokyo, Japan
[c] Department of Dermatology, National Defense Medical College, Saitama, Japan

ARTICLE INFO

Article history:
Received 17 October 2012
Received in revised form 21 January 2013
Accepted 31 January 2013

Keywords:
Aquaporin
Sweat gland
Trafficking
Anoctamin

ABSTRACT

Background: Aquaporin-5 (AQP5) is a member of the water channel protein family. Although AQP5 was shown to be present in sweat glands, the presence or absence of regulated intracellular translocation of AQP5 in sweat glands remained to be determined.
Objective: We investigated whether AQP5 in sweat glands translocated during sweating, and also sought to determine the intracellular signal that triggers this translocation.
Methods: Immunofluorescent analyses of AQP5 in mouse and human sweat glands were performed. Madin-Darby Canine kidney (MDCK) cell lines stably expressing human AQP5 were generated, and the regulated translocation of AQP5 in the polarized cells was assessed by immunofluorescent analysis and biotinylation assays.
Results: AQP5 showed rapid translocation to the apical membranes during sweating. In human eccrine sweat glands, immunoreactive AQP5 was detected in the apical membranes and the intercellular canaliculi of secretory coils, and in the basolateral membranes of the clear cells. Treatment of human AQP5-expressing MDCK cells with calcium ionophore A23187 resulted in a twofold increase of AQP5 in the apical membranes within 5 min.
Conclusion: The regulated AQP5 translocation may contribute to sweat secretion by increasing the water permeability of apical plasma membranes of sweat glands.

1. Introduction

Secretion of fluid is the principal function of eccrine sweat glands. An eccrine sweat gland is a single tubular structure consisting of a secretory portion and a ductal portion. In the secretory portion, primary fluid, i.e., primary sweat, is secreted onto the lumen by active salt transport followed by movement of water, and the fluid transits through the duct where salt reabsorption occurs [1,2]. Dyshidrosis, including hyperhidrosis, hypohidrosis and anhidrosis, is a serious problem that can have a severe impact on daily life. For example, primary focal hyperhidrosis is a disorder of excessive sweating that occurs in the palms, soles, axillae and craniofacial region. This condition results in occupational, psychological and physical impairment and potential social stigmatization [3,4]. Patients have several treatment options [5], but these treatments have complications and limitations [6]. Patients with obstinate dyshidrosis or who experience serious side effects are desperate for new treatments. In order to develop new treatments, further understanding of the regulation of sweating, especially the regulation of fluid movement, is required.

Aquaporins (AQPs) are a family of integral membrane channel proteins that allow the rapid movement of water across the plasma membrane. Thirteen members of the AQP family (AQP0–AQP12) have been identified in mammals to date, and these proteins are expressed in various fluid-transporting epithelia with a distinct tissue-specific pattern [7]. Although there have been a few reports regarding the presence of AQP5 in sweat glands [8–13], its involvement in sweating is not well understood.

In the present study, we focused on translocation of AQP5 in sweat glands. By immunofluorescent studies of AQP5 in the sweat glands, we found that AQP5 showed apical translocation during sweating. We then generated Madin-Darby canine kidney (MDCK) cell lines stably expressing human AQP5 (hAQP5), and found that the intracellular calcium might mediate this translocation.

* Corresponding author at: 1-5-45 Yushima, Bunkyo-ku, Tokyo 113-8510, Japan. Tel.: +81 3 5803 5214; fax: +81 3 5803 5215.
E-mail address: suchida.kid@tmd.ac.jp (S. Uchida).

0923-1811/$36.00
http://dx.doi.org/10.1016/j.jdermsci.2013.01.013

2. Materials and methods

2.1. Antibodies and chemical reagents

Primary antibodies used were: rabbit monoclonal anti-AQP5 (ab93230, Abcam, Cambridge, MA, USA), goat polyclonal anti-AQP5 (sc-9890, Santa Cruz Biotechnology, CA, USA), mouse monoclonal anti-Na^+/K^+ATPase (sc-21712, Sigma–Aldrich, St. Louis, MO, USA), and rabbit anti-anoctamin-1 (ANO1) antibody generated in our laboratory using the antigen peptide (NH_2–C + GDGSPVPSYEYHGDAL–COOH, corresponding to amino acid residues 941–956 of mouse ANO1). Secondary antibodies used for immunofluorescence were Alexa Fluor 488- or 546-conjugated anti-IgG antibodies (Invitrogen, Carlsbad, CA, USA). Alkaline phosphatase-conjugated anti-rabbit IgG antibody (S373B, Promega, Madison, WI, USA) was used as the secondary antibody for immunoblotting.

2.2. Animal study

We used C57BL6/J mice at the age of 24 weeks. Sweating was detected using a modified Minor method; mouse paws were painted with 3% iodine in ethanol, coated with 80% starch solution in olive oil and observed. To make the mice sweat, we simply held the mice in our hands without anesthesia. To obtain non-sweating mice, we intraperitoneally anesthetized the mice with Inactin (Dainippon Sumitomo Pharma, Osaka, Japan). In the sweating group, we could see spots appearing on their paws soon after holding. When the number and the size of the spots were still increasing (5 min after we started holding), the mice were rapidly anesthetized with diethyl ether (Sigma–Aldrich), and the paws of the mice in both groups were quickly removed and frozen in liquid nitrogen. All procedures and experiments were designed according to the Declaration of Helsinki Principles and approved by the Animal Care and Use Committee of Tokyo Medical and Dental University.

2.3. Immunofluorescence studies in mouse and human sweat glands

Specimens of healthy skin were taken from patients after surgery under local anesthesia with informed consent in accordance with the declaration of Helsinki Principles. The ethical committee of Tokyo Medical and Dental University approved this study. The specimens were fixed overnight in 10% Formalin Neutral Buffer Solution (Wako, Osaka, Japan) and embedded in paraffin. After antigen retrieval and blocking with 1% BSA, the sections were incubated overnight with primary antibodies. Immunofluorescent images were obtained by using an LSM confocal microscope (Carl Zeiss Japan, Tokyo, Japan). For quantification of AQP5 labeling, we evaluated the intensity of AQP5 immunofluorescence in each cross section of the coils using LSM5 software version 4.0. The percentage of AQP5 signal in the apical membranes to total signal in each coil was calculated.

2.4. Generation of MDCK cell lines stably expressing non-tagged human AQP5

hAQP5 cDNA without any tag sequence was amplified by PCR using hAQP5 cDNA in pDNOR201 (FLJ81272AAAF, NITE Biological Resource Center, Chiba, Japan) as a template, and was then subcloned into the pcDNA3.1 (+) vector (Invitrogen). Stably transfected MDCK cell clones were isolated in a selection medium containing 1.2 mg/ml G418 (Sigma–Aldrich) and screened by Western blot analysis using the anti-human AQP5 antibody.

2.5. Immunoblotting

The cells were lysed in a lysis buffer (1% Triton X-100, 50 mM Tris–HCl, 5 mM EDTA, 150 mM NaCl) for 30 min at 37 °C, and mixed with 2× Laemmli sample buffer for 15 min at room temperature to denature the proteins. The samples were run on a 10–20% SDS–PAGE gel (Wako) and blotted onto nitrocellulose membranes (RPN2020D, Amersham, Buckinghamshire, UK). Signals were detected using the WesternBlue chromogenic substrate (Promega).

2.6. Side-specific biotinylation assay

MDCK cells stably expressing hAQP5 were seeded on polycarbonate filters (Corning, NY, USA) until they formed a confluent monolayer. After treatment with or without 10 μM calcium ionophore A23187, Sulfo-NHS-Biotin (0.5 mg/ml) (Thermo Scientific, Waltham, MA, USA) was applied to the apical or the basolateral surface for 20 min. The subsequent procedures are described in our previous paper [14]. When side-specific biotinylated AQP5 protein was analyzed, an immunoreaction-enhancing solution (NKB101, TOYOBO, Osaka, Japan) was used. Band intensity was analyzed using Image J (NIH, Bethesda, MD, USA).

2.7. Statistical methods

Statistical analyses were performed using the Student's *t*-test. $P < 0.05$ was considered statistically significant.

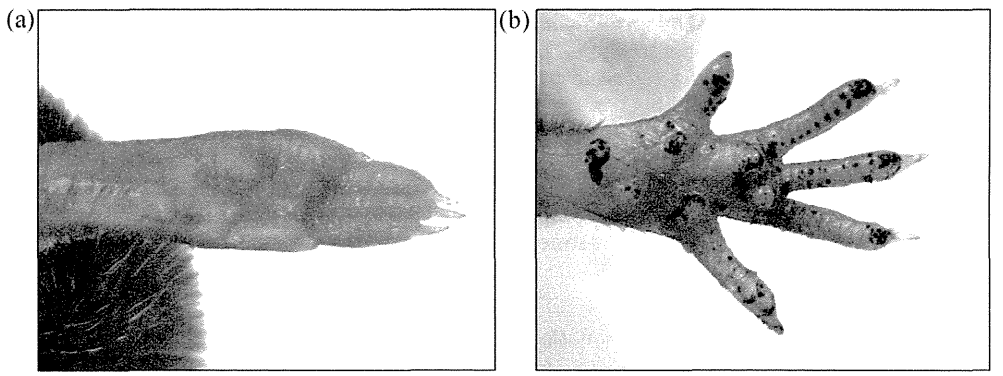

Fig. 1. Confirmation of non-sweating/sweating of mice through their paws. Representative photographs of the paw of a non-sweating/sweating mouse are shown. (a) No spot corresponding to sweat secretion was apparent on the paw of an anesthetized mouse. (b) Numerous spots were observed on the paw of a mouse which was held in the hand without anesthesia.

3. Results

3.1. AQP5 translocated from the non-apical region to the apical membranes in cells of mouse sweat glands under sweating condition

AQP5 was reported to translocate to the apical membranes of cells of rat parotid glands with cevimeline, a muscarinic receptor agonist [15]. We therefore assessed changes in the subcellular localization of AQP5 in sweat glands during sweating in mice. To determine whether the mice were sweating or not through their paws, we used a modified Minor method. In the control anesthetized mice, spots which correspond to sweat secretion, were scarcely observed on the paws (Fig. 1a). To make the mice sweat, we chose to simply hold the mice in our hands without anesthesia, rather than to apply a sweating agent such as pilocarpine or acetylcholine, since more spots were observed on the paws of the held mice than the mice given sweating agents (Fig. S1). After confirming that the mice were in non-sweating or sweating condition, the paws were removed and processed for immunofluorescence. Under non-sweating condition, AQP5 was detected in the apical membranes of secretory cells in the mouse sweat glands, and was diffusely localized in the non-apical region

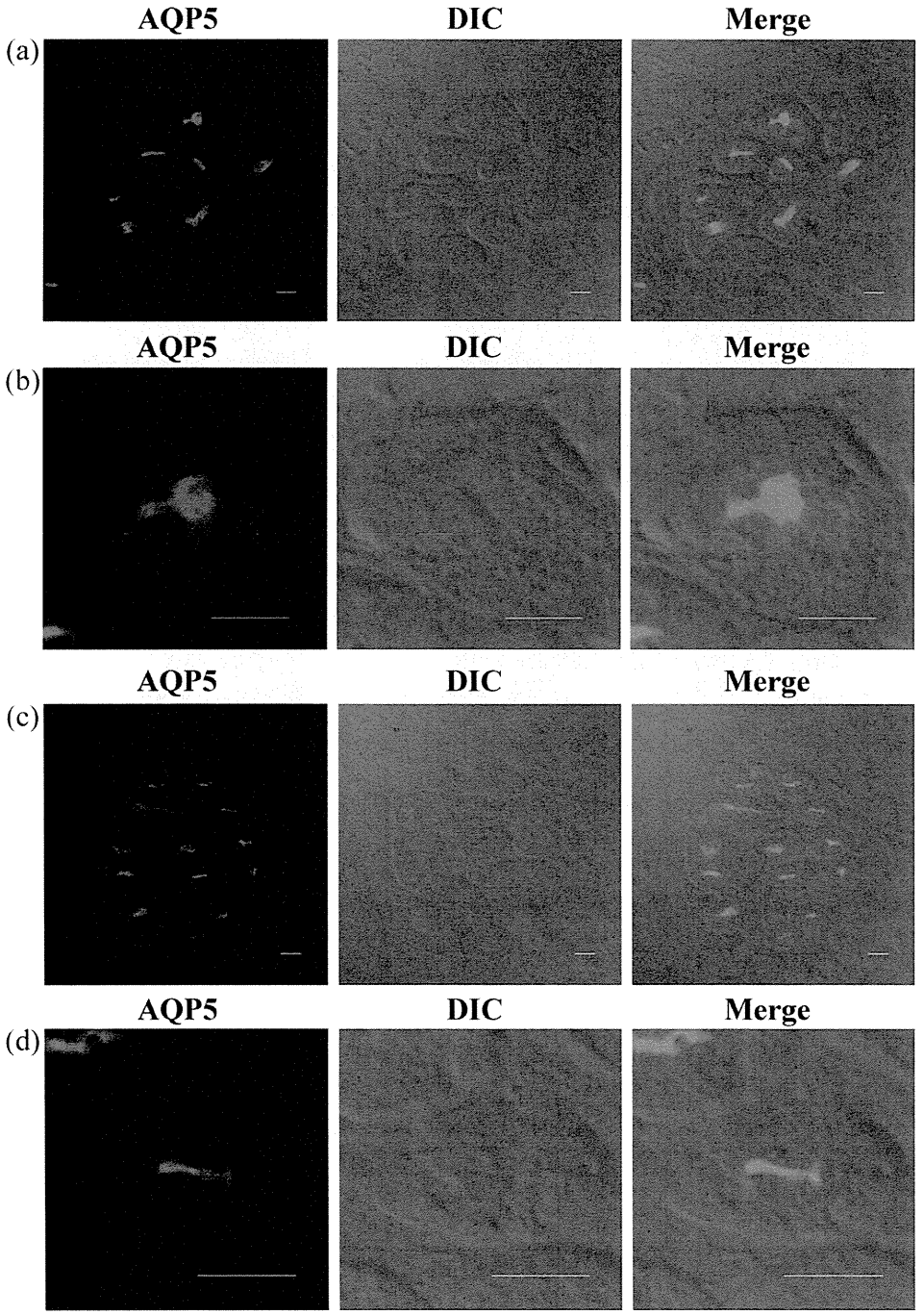

Fig. 2. Aquaporin-5 (AQP5) translocation from the non-apical region to the apical membranes of cells in mouse sweat glands. (a–d) Immunofluorescent staining of AQP5 localization in paraffin sections of a representative mouse sweat gland under non-sweating or sweating conditions. (a and b) Under non-sweating condition, immunoreactive AQP5 was detected in the apical membranes as well as in the non-apical region of the secretory cells. (c and d) Under sweating condition, almost all immunoreactive AQP5 was detected in the apical membranes. Bar = 10 μm.

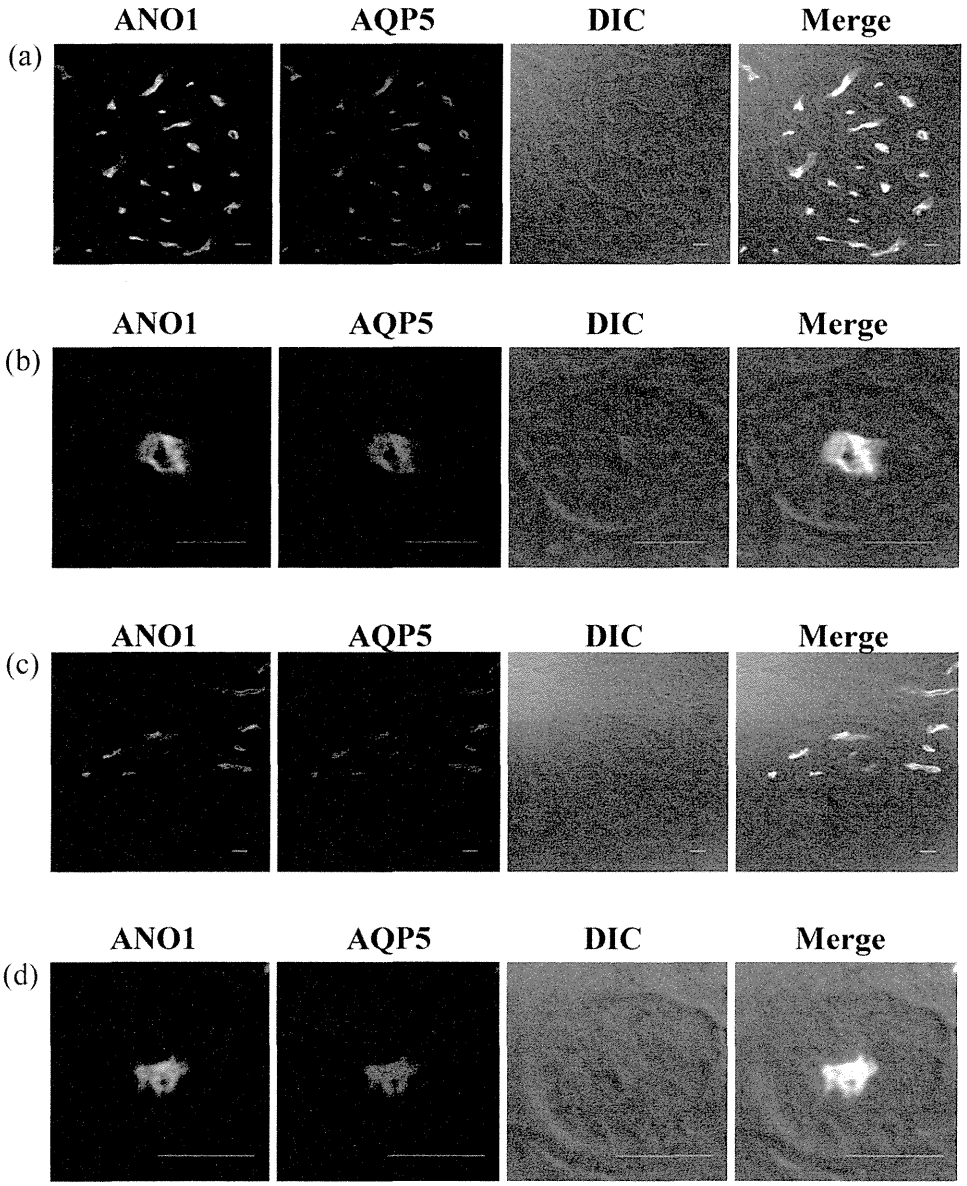

Fig. 3. Colocalization of anoctamin-1 (ANO1) and AQP5 in mouse sweat glands. Double immunofluorescent staining of ANO1 (green) and AQP5 (red) in histological sections of the paw of a representative mouse under non-sweating or sweating condition are shown. (a and b) Under non-sweating condition, immunoreactive ANO1 was detected in the apical membranes of the secretory cells and partially colocalized with AQP5. (c and d) Under sweating condition, immunoreactive ANO1 was detected in the apical membranes of these cells and colocalized with AQP5 in the apical membranes. The cellular localization of ANO1 did not change during sweating. Bar = 10 μm.

(Fig. 2a and b). Under sweating condition, almost all AQP5 staining was detected in the apical membranes (Fig. 2c and d). This apical accumulation of AQP5 was also confirmed in the pilocarpine-induced sweating (Fig. S1). The fluorescent intensity in the apical AQP5 in the cross section of the coils was significantly increased from 60 ± 7.7% (n = 15) under non-sweating condition to 91 ± 6.0% (n = 15) under sweating condition (mean ± SD, $P < 0.01$). These data suggested that a certain amount of AQP5 translocated from the non-apical region to the apical membranes during sweating.

Supplementary material related to this article found, in the online version, at http://dx.doi.org/10.1016/j.jdermsci.2013.01.013.

To exclude the possibility that translocation of AQP5 to the apical membranes is a general characteristic of apical membrane proteins in sweat glands during sweating, we investigated the localization of anoctamin-1 (ANO1), a calcium-activated chloride channel [16–18], during sweating. ANO1 immunofluorescence was detected in the apical membranes of cells in mouse sweat glands (Fig. S2). We then performed double immunofluorescent analysis of ANO1 and AQP5 in histological sections of the mice paws under non-sweating and sweating conditions. ANO1 was detected only in the apical membranes under both conditions, and it completely colocalized with AQP5 in these apical membranes (Fig. 3). However, in contrast to AQP5, the localization of ANO1 did not differ under the different applied conditions.

Supplementary material related to this article found, in the online version, at http://dx.doi.org/10.1016/j.jdermsci.2013.01.013.

3.2. Immunohistochemical analysis of AQP5 localization in human eccrine sweat glands

To determine the cellular localization of AQP5 in human eccrine sweat glands, we immunohistochemically analyzed paraffin sections of healthy human skin using the anti-AQP5 antibody. In addition, the anti-Na^+/K^+ATPase antibody was used for visualizing

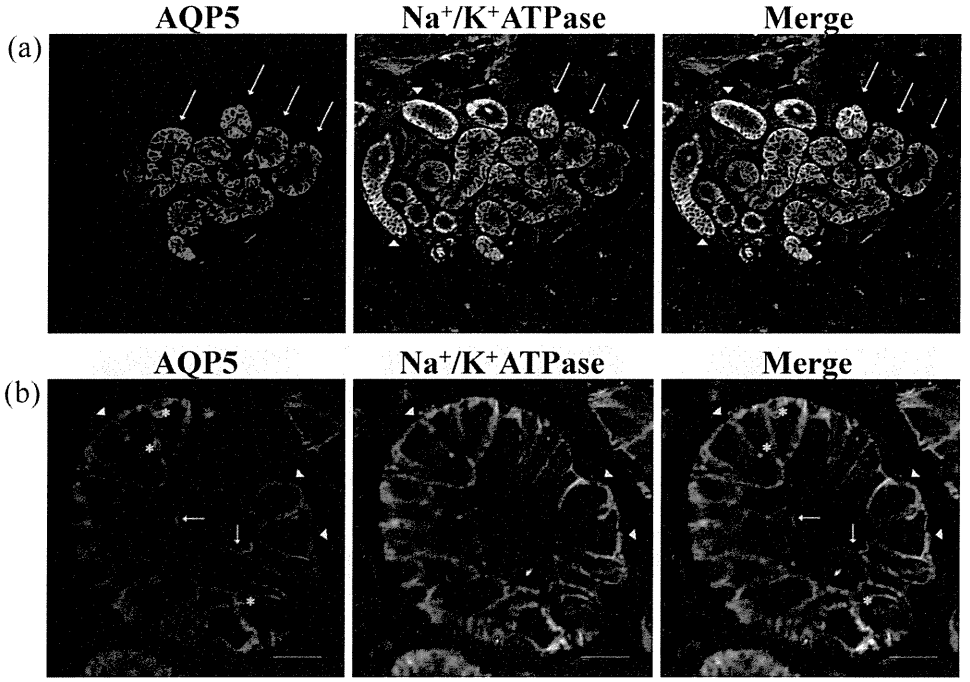

Fig. 4. Immunohistochemical analysis of AQP5 localization in human eccrine sweat glands. (a) Representative double immunofluorescent staining of AQP5 (red) and Na^+/K^+ATPase (green) in a paraffin section of a human eccrine sweat gland. Immunoreactive AQP5 was detected in cells of the secretory portion of the gland (arrows), but not in duct cells (arrowheads). (b) Close up images of the secretary coil of a human eccrine sweat gland. Immunoreactive AQP5 was detected in the apical membranes (arrows) and in the intercellular canaliculi (asterisks), and did not colocalize with Na^+/K^+ATPase in these areas. AQP5 was also detected in the basolateral membranes of the clear cells (arrowheads) where it did colocalize with Na^+/K^+ATPase. Bar = 10 μm.

the morphology of the eccrine sweat gland (Fig. 4). Immunoreactive AQP5 was detected in cells in the secretory portion of the eccrine sweat gland, but not in duct cells, whereas immunoreactive Na^+/K^+ATPase was detected in cells of both the secretory portion and the duct. Sweat gland duct cells showed strong Na^+/K^+ATPase labeling at their basolateral plasma membranes as previously reported [19,20], whereas cells in the secretory portion showed relatively weak labeling at their basolateral plasma membranes (Fig. 4a). AQP5 was detected in the apical membranes (Fig. 4b, arrows) of cells in the secretory portion as well as in the intercellular canaliculi (Fig. 4b, asterisks), and this AQP5 staining did not colocalize with Na^+/K^+ATPase staining. In addition, AQP5 was also detected in the basolateral membranes of the clear cells (Fig. 4b, arrowheads). Cytoplasmic staining of AQP5 as observed in mouse sweat glands was not observed in our specimens of human eccrine sweat glands. Analysis of different specimens of healthy skin from several patients using two other anti-AQP5 antibodies (sc-9890 and sc-28628, Santa Cruz Biotechnology) indicated almost exactly the same distribution of AQP5 shown in Fig. 4. AQP5 was not detected in other components of the skin, including the epidermis, sebaceous glands and hair follicles (data not shown).

3.3. Transfected human AQP5 is located at both the apical and basolateral membranes of MDCK cells

To further investigate AQP5 cellular localization and translocation, we generated MDCK cell lines stably expressing non-tagged hAQP5. The transfected hAQP5 was not tagged since some tag sequences are known to affect the cellular localization of AQP5 [21]. We selected nine clones from these transfected cells based on Western blotting of AQP5 protein expression (Fig. 5a). Of these clones, clone #6, which showed a high level of AQP5 expression, and a mixture of clones #4, #7 and #9, which was used to avoid the effect of clonal variation on the results, were selected for further experiments. In preliminary experiments, we confirmed that these cells formed a confluent monolayer and were in a polarized state by checking the basolateral localization of Na^+/K^+ATPase (data not shown). A cell-side-specific biotinylation assay showed that hAQP5 was present at both the apical and basolateral membranes of these cells (Fig. 5b), which was consistent with the immunohistochemical localization of AQP5 in human eccrine sweat glands in vivo (Fig. 4).

3.4. Human AQP5 translocated from the cytoplasm to the apical membranes by treatment with calcium ionophore

In rat parotid glands, the interaction of acetylcholine with M3 muscarinic receptors and of norepinephrine with α1-adrenergic receptors stimulates salivary secretion by inducing an elevation of intracellular calcium concentration and the translocation of rat AQP5 from the intracellular membranes to the apical membranes [22,23]. Sweating is also primarily regulated by

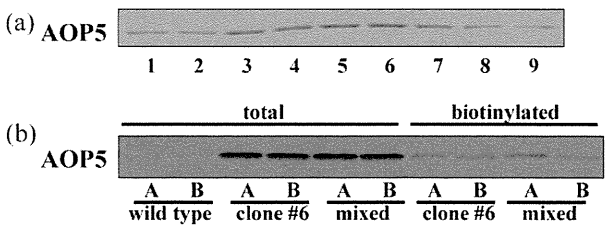

Fig. 5. Analysis of MDCK cell lines stably expressing non-tagged hAQP5. (a) Nine independent clones were isolated and their expression of hAQP5 was analyzed by Western blotting. Clone #6, which showed a high level of AQP5 expression, and a mixture of clones #4, #7 and #9, which was used to avoid the effect of clonal variation, were selected for further experiments. (b) Localization of hAQP5 in the stable cell lines was determined by a cell-side-specific biotinylation assay. The hAQP5 was detected at both the apical and basolateral sides of polarized hAQP5-MDCK cells. A, apical membrane fraction; B, basolateral membrane fraction; wild-type, wild-type MDCK cell line; mixed, mixed clone of #4, #7 and #9.

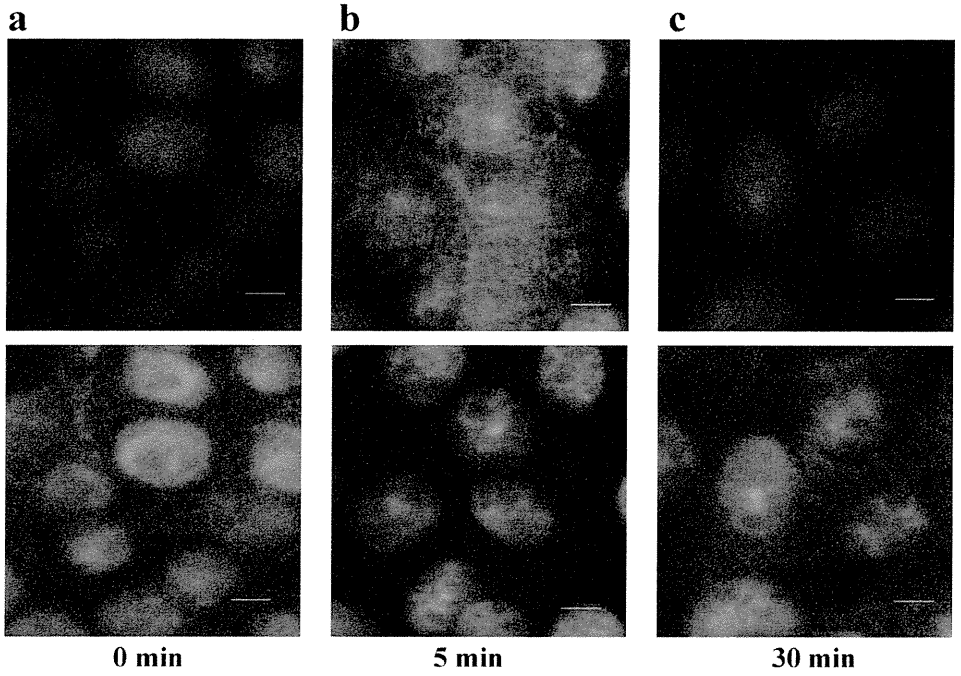

Fig. 6. Immunofluorescent analysis of human AQP5 translocation to the apical membranes of MDCK cells. Confocal images of hAQP5 in MDCK cells (clone #6) treated with 10 μM A23187. The top and bottom images show hAQP5 at the apical surface and the nucleus levels of the monolayers, respectively. hAQP5 at the apical surface level was increased 5 min after treatment. Red: AQP5, blue: 4,6-diamidino-2-phenylindole (DAPI). Bar = 5 μm.

acetylcholine, which causes an increase in intracellular calcium concentration via muscarinic receptors [1]. We therefore tried to determine whether hAQP5 translocation was regulated by an increase in intracellular calcium concentration in MDCK cells stably expressing non-tagged hAQP5. Confluent monolayers of the hAQP5-MDCK cells were treated with or without (control) 10 μM calcium ionophore A23187 for 5 or 30 min and were then subjected to an immunofluorescent analysis and a cell-side-specific biotinylation assay. In both analyses, the amount of hAQP5 protein in the apical membrane fraction increased after 5 min of A23187 treatment compared to control cells (Figs. 6 and 7a and e), and it returned to the control level 30 min after this treatment (Figs. 6 and 7b and f). On the other hand, the amount of hAQP5 protein in the basolateral membrane fraction did not change at either 5 or 30 min after treatment (Fig. 7c, d, g and h). The same results were obtained using 20 μM thapsigargin, another reagent that increases intracellular calcium concentration (data not shown). These results suggest that hAQP5 protein translocated relatively rapidly from the cytoplasm to the apical membranes due to an increase in intracellular calcium.

4. Discussion

AQP5 water channel is expressed in several secretory epithelia, including salivary glands [24], airway submucosal glands [25], lacrimal glands [26], and sweat glands, as well as in alveolar type I epithelial cells [25,27]. Aquaporin-2 (AQP2) is a water channel in the collecting ducts of the kidney that translocates from intracellular membranes to plasma membranes in response to vasopressin [28–30]. AQP5 has 63% identity to AQP2 [31], and was shown to translocate from the cytoplasm to the apical membranes in cells of rat salivary glands by stimulation with M3 muscarinic and α1-adrenergic agonists [22,23]. However, there has been no report regarding AQP5 translocation in cells of sweat glands. Since it was difficult to investigate the mechanism of AQP5 translocation in human tissues, we first used mouse tissues for this investigation. We observed the significant decrease of mouse AQP5 in the non-apical region and its accumulation in the apical membranes under sweating condition (Fig. 2). This is the first report of AQP5 translocation in sweat glands in vivo.

In human samples, however, we could not observe apparent cytoplasmic AQP5 signals (Fig. 4). We speculate that the patients undergoing biopsy were under emotional sweating condition due to mental strain. To verify this speculation, the specimen of anhidrotic skin, for example, skin from the patients who had underwent sympathectomy, may be necessary.

We consider that apical translocation is not a general characteristic of apical membrane proteins involved in sweating since we could not observe the translocation of ANO1 in the same sections (Fig. 3). ANO1 is the first member of a family of calcium-activated chloride channels that were recently identified as anoctamins [16–18]. Although calcium-activated chloride channels have been postulated to be involved in sweating, the presence of anoctamins in sweat glands has not been reported. We believe that this is the first report to clearly demonstrate ANO1 apical membrane localization in sweat glands and to show that ANO1 does not translocate during sweating. Since the function of ANO1 is regulated by calcium, it is reasonable to presume that ANO1 does not need to traffic within the cell for its function. Thus, the findings of the present study, i.e., that AQP5 colocalizes with ANO1 in sweat glands, and that AQP5 translocates during sweating, provide new insights into the mechanism by which primary sweat is produced.

We could detect human AQP5 signals in the basolateral membranes as well as in the apical membranes (Fig. 4). There must be high water permeability in both apical and basolateral plasma membranes for tight epithelia to be highly permeable to water. In kidney collecting ducts, there are AQP3 and AQP4 in the basolateral plasma membranes, which make the membranes constitutively permeable to water. The trafficking of AQP2 to the apical membranes is the key machinery to increase transepithelial water permeability by vasopressin signal. We speculate that basolateral AQP5 in sweat glands may have the same role as AQP3 and AQP4 in the collecting ducts.

The principal regulator of sweat secretion in primates and rodents is acetylcholine [1,32], whose effects are mediated by the

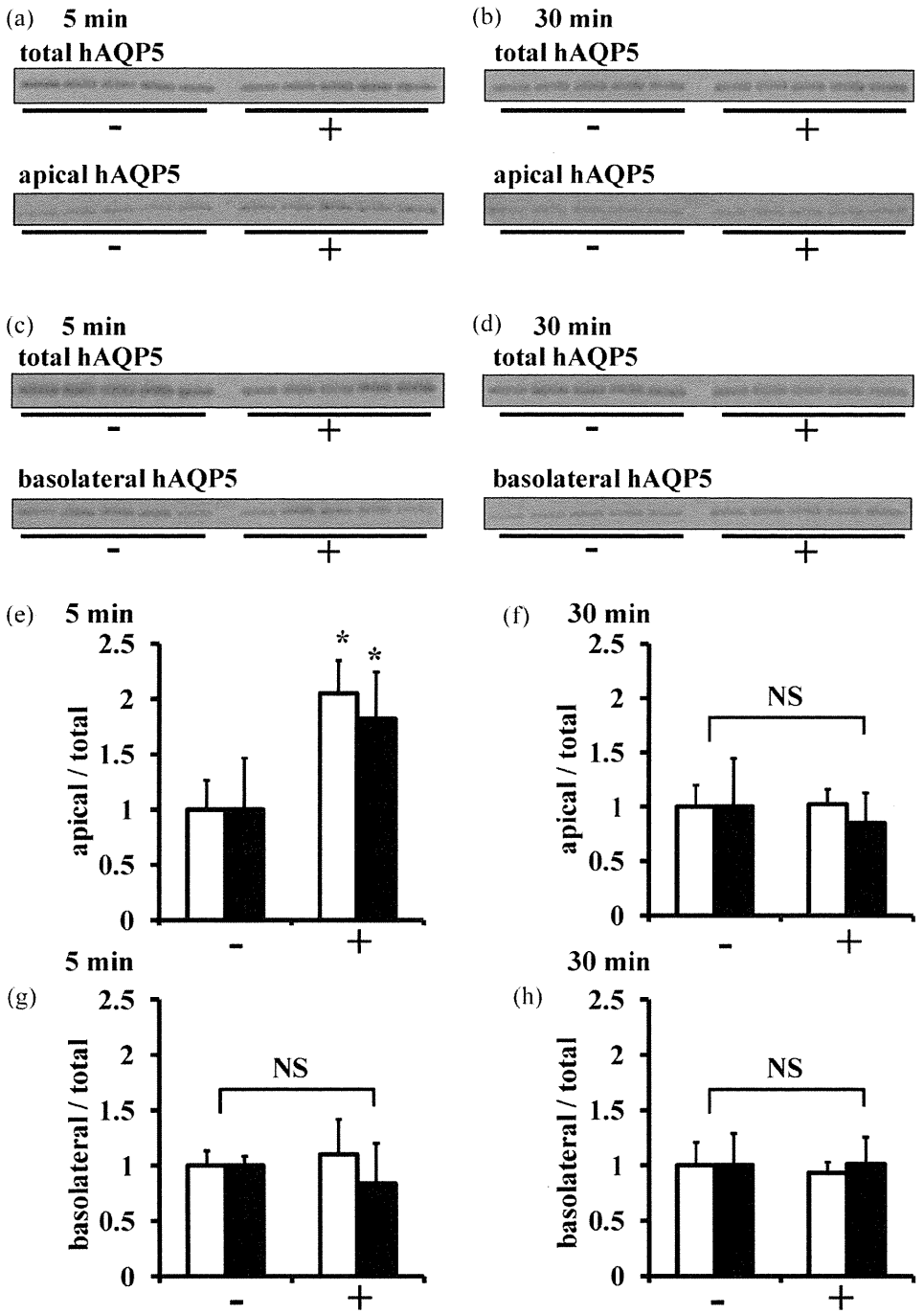

Fig. 7. Human AQP5 translocation from the cytoplasm to the apical membranes of MDCK cells. (a–d) Confluent monolayers of the hAQP5-MDCK cells were treated with or without (control) 10 μM calcium ionophore A23187 and then subjected to a cell-side-specific biotinylation assay. The figures are representative results using clone #6. (e–h) Densitometric analysis of (a–d) and the results using mixed clone. After 5 min of the treatment (a and e), the apical hAQP5 level increased by about twofold in A23187-treated cells, and after 30 min of the treatment (b and f), it returned to the control level. The basolateral hAQP5 level did not change after 5 or 30 min of the treatment (c, d, g, h). White bars, clone #6 ($n = 5$); black bars, mixed clone ($n = 5$). Error bars indicate SD. *$P < 0.05$. NS; not significant.

intracellular second messenger calcium. We therefore tried to determine if human AQP5 translocation was mediated by intracellular calcium using a cell culture system. The signaling pathways that are involved in AQP5 trafficking in vitro have been investigated using several types of epithelial cells. Biochemical analysis of slices of rat parotid glands suggested that AQP5 is translocated from cytoplasmic compartments to the apical membrane fraction by stimulation of M3 muscarinic receptors and α1-adrenergic receptors [22,23]. Rat AQP5 in human salivary gland (HSG) cells was shown to undergo rapid translocation to plasma membranes by treatment with thapsigargin, an inhibitor of the endoplasmic Ca^{2+}ATPase or with calcium ionophore A23187 [33]. However, this study was not performed in the cells under polarized condition, and the translocation evaluated only by immunofluorescence appeared to be localized not to the apical but to the lateral plasma membranes [33]. Unlike rat AQP5 in parotid glands, human AQP5 is present both in the apical and basolateral plasma membranes in sweat glands (Fig. 4). Therefore, we thought that we should determine the translocation of human AQP5 in polarized cells. In addition, we used non-tagged AQP5 for our study since a previous report indicated that

the cellular behavior of AQP5, especially in terms of membrane trafficking in cell culture systems, appears to be significantly influenced by tag sequences attached to AQP5 [21]. Although we would have liked to perform this experiment in cells derived from an eccrine sweat gland, there is no such cells feasible for this type of experiment, so we used MDCK cells instead. MDCK cells form a polarized epithelial monolayer when grown on a permeable support [34,35], and have been one of the most useful model cells for the study of intracellular trafficking of molecules in epithelial cells.

hAQP5 localized both apically and basolaterally in all isolated stable clones of hAQP5-transfected MDCK cells with a similar pattern as that of AQP5 in human eccrine sweat glands in vivo. The observed behavior of non-tagged human AQP5 in these cell lines, i.e., rapid translocation only to the apical plasma membrane by A23187 and thapsigargin treatment, is also consistent with the translocation observed in vivo, clearly suggesting that intracellular calcium is an important regulator of apical AQP5 trafficking in sweating. At present, little is known about the molecular mechanism(s) of AQP5 trafficking by intracellular calcium. Unlike AQP2, whether AQP5 phosphorylation is involved in the mechanism(s) remains to be determined.

Regarding the role of AQP5 in sweat glands, the previous knockout mouse studies reported contradictory results: one study demonstrated dramatically reduced sweating in AQP5 null (−/−) mice [12], while the other study demonstrated no significant difference in sweating between wild-type mice and AQP5 null (−/−) mice [11]. The reason for this discrepancy is not clear at present. Our study clearly showed the existence of regulated apical translocation of AQP5 in sweat glands, which does not answer whether AQP5 is necessary for sweating or not, but suggests that AQP5 may contribute to sweat secretion by increasing the water permeability of apical plasma membranes of sweat glands.

In conclusion, we clearly demonstrated the rapid translocation of AQP5 to the apical plasma membranes during sweating and by the agents increasing intracellular calcium concentration. Agents that modulate AQP5 function may be useful for the treatment of patients with sweating disorders.

Funding sources

This study was supported by Health and Labor Sciences Research Grants from Ministry of Health, Labor and Welfare of Japan: Research on intractable diseases (Nos. 0309001, 1211202), Grant-in-Aid for Scientific Research (A) from the Japan Society for the Promotion of Science (Nos. 20249047, 22249032), Takeda Science Foundation, and Salt Science Research Foundation (1026).

Acknowledgments

We thank Chiyako Miyagishi and Motoko Chiga of Tokyo Medical and Dental University for excellent technical assistance.

References

[1] Sato K. The physiology, pharmacology, and biochemistry of the eccrine sweat gland. Rev Physiol Biochem Pharmacol 1997;79:51–131.
[2] Dobson RL, Sato K. The secretion of salt and water by the eccrine sweat gland. Arch Dermatol 1972;105:366–70.
[3] Swartling C, Naver H, Lindberg M. Botulinum A toxin improves life quality in severe primary focal hyperhidrosis. Eur J Neurol 2001;8:247–52.
[4] Cinà CS, Clase CM. The illness intrusiveness rating scale: a measure of severity in individuals with hyperhidrosis. Qual Life Res 1999;8:693–8.
[5] Hornberger J, Grimes K, Naumann M, Glaser DA, Lowe NJ, Naver H, et al. Multispecialty working group on the recognition, and treatment of primary focal hyperhidrosis, recognition, diagnosis, and treatment of primary focal hyperhidrosis. J Am Acad Dermatol 2004;51:274–86.
[6] Doolabh N, Horswell S, Williams M, Huber L, Prince S, Meyer DM, et al. Thoracoscopic sympathectomy for hyperhidrosis: indications and results. Ann Thorac Surg 2004;77:410–4 [discussion 414].
[7] Ishibashi K, Hara S, Kondo S. Aquaporin water channels in mammals. Clin Exp Nephrol 2009;13:107–17.
[8] Ma L, Huang YG, He H, Deng YC, Zhang HF, Che HL, et al. Postnatal expression and denervation induced up-regulation of aquaporin-5 protein in rat sweat gland. Cell Tissue Res 2007;329:25–33.
[9] Ma L, Huang YG, Deng YC, Tian JY, Rao ZR, Che HL, et al. Topiramate reduced sweat secretion and aquaporin-5 expression in sweat glands of mice. Life Sci 2007;80:2461–8.
[10] Kabashima K, Shimauchi T, Kobayashi M, Fukamachi S, Kawakami C, Ogata M, et al. Aberrant aquaporin 5 expression in the sweat gland in aquagenic wrinkling of the palms. J Am Acad Dermatol 2008;59:S28–32.
[11] Song Y, Sonawane N, Verkman AS. Localization of aquaporin-5 in sweat glands and functional analysis using knockout mice. J Physiol 2002;541:561–8.
[12] Nejsum LN, Kwon TH, Jensen UB, Fumagalli O, Frøkiaer J, Krane CM, et al. Functional requirement of aquaporin-5 in plasma membranes of sweat glands. Proc Natl Acad Sci USA 2002;99:511–6.
[13] Iizuka T, Suzuki T, Nakano K, Sueki H. Immunolocalization of aquaporin-5 in normal human skin and hypohidrotic skin diseases. J Dermatol 2012;39:344–9.
[14] Yui N, Okutsu R, Sohara E, Rai T, Ohta A, Noda Y, et al. FAPP2 is required for aquaporin-2 apical sorting at trans-Golgi network in polarized MDCK cells. Am J Physiol Cell Physiol 2009;297:C1389–96.
[15] Ishikawa Y, Yuan Z, Inoue N, Skowronski MT, Nakae Y, Shono M, et al. Identification of AQP5 in lipid rafts and its translocation to apical membranes by activation of M3 mAChRs in interlobular ducts of rat parotid gland. Am J Physiol Cell Physiol 2005;289:C1303–11.
[16] Caputo A, Caci E, Ferrera L, Pedemonte N, Barsanti C, Sondo E, et al. TMEM16A, a membrane protein associated with calcium-dependent chloride channel activity. Science 2008;322:590–4.
[17] Schroeder BC, Cheng T, Jan YN, Jan LY. Expression cloning of TMEM16A as a calcium-activated chloride channel subunit. Cell 2008;134:1019–29.
[18] Yang YD, Cho H, Koo JY, Tak MH, Cho Y, Shim WS, et al. TMEM16A confers receptor-activated calcium-dependent chloride conductance. Nature 2008;455:1210–5.
[19] Quinton PM, Tormey JM. Localization of Na/K-ATPase sites in the secretory and reabsorptive epithelia of perfused eccrine sweat glands: a question to the role of the enzyme in secretion. J Memb Biol 1976;29:383–99.
[20] Saga K, Sato K. Ultrastructural localization of ouabain-sensitive, K-dependent p-nitrophenyl phosphatase activity in monkey eccrine sweat gland. J Histochem Cytochem 1988;36:1023–30.
[21] Kosugi-Tanaka C, Li X, Yao C, Akamatsu T, Kanamori N, Hosoi K. Protein kinase A-regulated membrane trafficking of a green fluorescent protein-aquaporin 5 chimera in MDCK cells. Biochim Biophys Acta 2006;1763:337–44.
[22] Ishikawa Y, Eguchi T, Skowronski MT, Ishida H. Acetylcholine acts on M3 muscarinic receptors and induces the translocation of aquaporin5 water channel via cytosolic Ca^{2+} elevation in rat parotid glands. Biochem Biophys Res Commun 1998;245:835–40.
[23] Ishikawa Y, Skowronski MT, Inoue N, Ishida H. alpha(1)-adrenoceptor-induced trafficking of aquaporin-5 to the apical plasma membrane of rat parotid cells. Biochem Biophys Res Commun 1999;265:94–100.
[24] Ma T, Song Y, Gillespie A, Carlson EJ, Epstein CJ, Verkman AS. Defective secretion of saliva in transgenic mice lacking aquaporin-5 water channels. J Biol Chem 1999;274:20071–74.
[25] Nielsen S, King LS, Christensen BM, Agre P. Aquaporins in complex tissues. II. Subcellular distribution in respiratory and glandular tissues of rat. Am J Physiol 1997;273:C1549–61.
[26] Moore M, Ma T, Yang B, Verkman AS. Tear secretion by lacrimal glands in transgenic mice lacking water channels AQP1, AQP3, AQP4 and AQP5. Exp Eye Res 2000;70:557–62.
[27] Dobbs LG, Gonzalez R, Matthay MA, Carter EP, Allen L, Verkman AS. Highly water-permeable type I alveolar epithelial cells confer high water permeability between the airspace and vasculature in rat lung. Proc Natl Acad Sci USA 1998;95:2991–6.
[28] Yamamoto T, Sasaki S, Fushimi K, Ishibashi K, Yaoita E, Kawasaki K. Vasopressin increases AQP-CD water channel in apical membrane of collecting duct cells in Brattleboro rats. Am J Physiol 1995;268:C1546–51.
[29] Nielsen S, DiGiovanni SR, Christensen EI, Knepper MA, Harris HW. Cellular and subcellular immunolocalization of vasopressin-regulated water channel in rat kidney. Proc Natl Acad Sci USA 1993;90:11663–67.
[30] Fushimi K, Uchida S, Hara Y, Hirata Y, Marumo F, Sasaki S. Cloning and expression of apical membrane water channel of rat kidney collecting tubule. Nature 1993;361:549–52.
[31] Raina S, Preston GM, Guggino WB, Agre P. Molecular cloning and characterization of an aquaporin cDNA from salivary, lacrimal, and respiratory tissues. J Biol Chem 1995;270:1908–12.
[32] Sato K, Cavallin S, Sato KT, Sato F. Secretion of ions and pharmacological responsiveness in the mouse paw sweat gland. Clin Sci (Lond) 1994;86:133–9.
[33] Tada J, Sawa T, Yamanaka N, Shono M, Akamatsu T, Tsumura K, et al. Involvement of vesicle–cytoskeleton interaction in AQP5 trafficking in AQP5-gene-transfected HSG cells. Biochem Biophys Res Commun 1999;266:443–7.
[34] Cereijido M, Robbins ES, Dolan WJ, Rotunno CA, Sabatini DD. Polarized monolayers formed by epithelial cells on a permeable and translucent support. J Cell Biol 1978;77:853–80.
[35] Misfeldt DS, Hamamoto ST, Pitelka DR. Transepithelial transport in cell culture. Proc Natl Acad Sci USA 1976;73:1212–6.

BJ ChemBio

Biochem. J. (2013) **455**, 339–345 (Printed in Great Britain) doi:10.1042/BJ20130597

online data

Chemical library screening for WNK signalling inhibitors using fluorescence correlation spectroscopy

Takayasu MORI*, Eriko KIKUCHI*, Yuko WATANABE†, Shinya FUJII†, Mari ISHIGAMI-YUASA‡, Hiroyuki KAGECHIKA†‡, Eisei SOHARA*, Tatemitsu RAI*, Sei SASAKI* and Shinichi UCHIDA*[1]

*Department of Nephrology, Graduate School of Medical and Dental Sciences, Tokyo Medical and Dental University, 1-5-45 Yushima, Bunkyo, Tokyo 113-8519, Japan, †Institute of Biomaterials and Bioengineering, Tokyo Medical and Dental University, 1-5-45 Yushima, Bunkyo, Tokyo 113-8519, Japan, and ‡Chemical Biology Screening Center, Tokyo Medical and Dental University, 1-5-45 Yushima, Bunkyo, Tokyo, 113-8519, Japan

WNKs (with-no-lysine kinases) are the causative genes of a hereditary hypertensive disease, PHAII (pseudohypoaldosteronism type II), and form a signal cascade with OSR1 (oxidative stress-responsive 1)/SPAK (STE20/SPS1-related proline/alanine-rich protein kinase) and Slc12a (solute carrier family 12) transporters. We have shown that this signal cascade regulates blood pressure by controlling vascular tone as well as renal NaCl excretion. Therefore agents that inhibit this signal cascade could be a new class of antihypertensive drugs. Since the binding of WNK to OSR1/SPAK kinases was postulated to be important for signal transduction, we sought to discover inhibitors of WNK/SPAK binding by screening chemical compounds that disrupt the binding. For this purpose, we developed a high-throughput screening method using fluorescent correlation spectroscopy. As a result of screening 17000 compounds, we discovered two novel compounds that reproducibly disrupted the binding of WNK to SPAK. Both compounds mediated dose-dependent inhibition of hypotonicity-induced activation of WNK, namely the phosphorylation of SPAK and its downstream transporters NKCC1 (Na/K/Cl cotransporter 1) and NCC (NaCl cotransporter) in cultured cell lines. The two compounds could be the promising seeds of new types of antihypertensive drugs, and the method that we developed could be applied as a general screening method to identify compounds that disrupt the binding of two molecules.

Key words: chemical library, fluorescent correlation spectroscopy, hypertension, Na/Cl cotransporter, WNK.

INTRODUCTION

PHAII (pseudohypoaldosteronism type II) is an autosomal dominant hereditary hypertensive disease characterized by hyperkalaemia and metabolic acidosis [1]. WNK1 (with-no-lysine kinase 1) and WNK4 were identified as the genes responsible for PHAII [2]. Since the discovery of mutations in the WNK1 and WNK4 genes in PHAII, the role of WNKs in the regulation of transporters and channels has been studied in order to elucidate the pathogenic mechanisms of PHAII [3–6]. On the basis of these observations, WNKs have been attracting attention as new factors controlling human blood pressure. We previously generated Wnk4D561A/+ knock-in mice carrying a heterozygous D561A missense mutation in the *Wnk4* gene, which corresponds to the D564A mutation found in PHAII patients [7], and found increased phosphorylation of the NCC (NaCl cotransporter) and OSR1 (oxidative stress-responsive 1) and SPAK (STE20/SPS1-related proline/alanine-rich protein kinase), which are substrates of WNKs [7–9]. The increased phosphorylation and activation of NCC caused excessive sodium reabsorption in the distal convoluted tubules in the kidney, which contributes to salt-sensitive hypertension. Previously, the NKCC1 (Na/K/Cl cotransporter 1) phosphorylation cascade in vascular smooth muscle cells was also found to be important for the regulation of vascular tonus [10–12]. Furthermore, WNK signalling was positively regulated by aldosterone [9], angiotensin II [13,14] and insulin [15,16]. Therefore agents that inhibit this signal cascade could form a new class of antihypertensive drugs that may have dual diuretic and vasodilator effects and might be particularly effective in patients with hyperaldosteronism or hyperinsulinaemia [16,17]. Protein–protein interactions are of great interest as a tool for drug discovery [18–21]. To develop WNK signalling inhibitors, we focused on a known binding motif present in both WNK and OSR1/SPAK [22]. In the present study, we sought to discover such drugs by screening chemical compounds that disrupt binding and control signalling. For this purpose, we developed a high-throughput screening method that uses FCS (fluorescent correlation spectroscopy).

MATERIALS AND METHODS

Cell culture and inhibition assay

The murine distal convoluted tubule cell line (mpkDCT) provided by Dr A. Vandewalle (INSERM U773, Université Paris, Paris, France) was cultured in a defined medium as described previously [23]. MOVAS (mouse vascular smooth muscle) cells were cultured in DMEM (Dulbecco's modified Eagle's medium) supplemented with 10% (v/v) FBS, 2 mM L-glutamine, 100 units/ml penicillin and 0.1 mg/ml streptomycin at 37 °C in a humidified 5% CO_2 incubator. mpkDCT cells and MOVAS cells were cultured in six-well dishes. Cells were exposed to various concentrations of compounds for 20 min and stimulated with hypotonic low-chloride medium [24] for 45 min. Cells were lysed by the addition of 0.15 ml of ice-cold lysis buffer [50 mM Tris/HCl, pH 7.5, 150 mM NaCl, 1 mM EGTA, 1 mM EDTA, 50 mM sodium fluoride, 1 mM sodium orthovanadate, 1% Triton X-100, 0.27 M sucrose, 1 mM DTT and Complete™ protease

Abbreviations used: FCS, fluorescent correlation spectroscopy; MOVAS, mouse vascular smooth muscle; NCC, NaCl cotransporter; NKCC1, Na/K/Cl cotransporter 1; OSR1, oxidative stress-responsive 1; PHAII, pseudohypoaldosteronism type II; SPAK, STE20/SPS1-related proline/alanine rich protein kinase; TAMRA, 6-carboxytetramethylrhodamine; WNK, with-no-lysine kinase.

[1] To whom correspondence should be addressed (email suchida.kid@tmd.ac.jp).

inhibitor cocktail (Roche) (1 tablet per 50 ml)] to each well. After centrifugation at 12000 *g* for 5 min at 4 °C, the supernatants were denatured for 20 min at 60 °C with SDS sample buffer (Cosmo Bio) and subjected to SDS/PAGE.

Immunoblotting

Quantitative immunoblotting was performed as described previously [7]. Blots were probed with the following primary antibodies: anti-(total NCC) [25], anti-phospho-NCC (pThr^{53}) [9], anti-(total NKCC1) (Hybridoma Bank), anti-phospho-NKCC1 [26], anti-(total SPAK) (Cell Signaling Technology), anti-phospho-SPAK [26] and anti-GAPDH (glyceraldehyde-3-phosphate dehydrogenase; Santa Cruz Biotechnology) antibodies. Alkaline phosphatase-conjugated anti-IgG antibodies (Promega) were used as secondary antibodies for immunoblotting. The intensities of the bands were analysed and quantified by ImageJ (NIH) software.

Expression and purification of GST–SPAK-CCT in *Escherichia coli*

The DNA encoding the residues 452–553 of rat SPAK (CCT, almost identical to residues 442–545 of human SPAK) was cloned into pGEX6P-1 vector. Recombinant GST-fusion SPAK (GST–SPAK-CCT) protein was expressed in BL21 *E. coli* cells, and 1 litre cultures were grown at 37 °C in 2YT broth [1.6 % (w/v) tryptone/1 % (w/v) yeast extract/0.5 % NaCl] containing 100 μg/ml ampicillin until the attenuance at 600 nm was 0.6. IPTG (1 mM) was then added, and the cells were cultured for an additional 16 h at 28 °C. Cells were isolated by centrifugation and resuspended in 40 ml of ice-cold PBS, followed by sonication (TOMY Ultrasonic Disrupters UD-201). Lysates were centrifuged at 4 °C for 5 min at 10000 *g*. The GST-fusion proteins were affinity purified on 1.2 ml glutathione–Sepharose beads and eluted in elution buffer containing 83 mM Tris/HCl, 150 mM KOH and 30 mM glutathione.

FCS

Fluorescent TAMRA (6-carboxytetramethylrhodamine)-labelled WNK4 peptide covering the RFQV motif [WNK4-RFQV (TAMRA-SEEGKPQLVGRFQVTSSK)], TAMRA-labelled WNK4 peptide in which the RFXV motif was mutated [WNK4-AFQV (TAMRA-SEEGKPQLVGA-FQVTSSK)], and TAMRA-labelled NCC peptide covering the RFTI motif [NCC-RFTI (TAMRA-TPGDATLCSGRFTISTLL)] were prepared (Hokkaido System Science). Recombinant GST–SPAK-CCT was expressed in BL21 *E. coli* cells and purified using glutathione–Sepharose beads. The TAMRA-labelled peptides were incubated at room temperature (25 °C) for 30 min with various concentrations of GST–SPAK-CCT (1–65 μM) in 1×PBS with 0.05 % Tween 20 reaction buffer, and the FCS measurements of single-molecule fluorescence were performed using the FluoroPoint-light analytical system (Olympus) [27]. The confocal volume to detect fluorescent signals in this equipment is in the range of a single femtolitre. Therefore TAMRA-labelled peptide was diluted so that a single fluorophore was likely to be present in the confocal space. The final concentration of each peptide in the FCS assays was 2.7 nM. The concentration of GST–SPAK-CCT used for screening was 0.5 μM, since at this concentration the binding reaction was not saturated and reproducibly detected (see Figure 1A). The concentration of DMSO used as a solvent of compounds was 1 % in the final assay solutions.

The assay was performed in a 384-well plate. All experiments were performed in 15 s of data acquisition time, and the

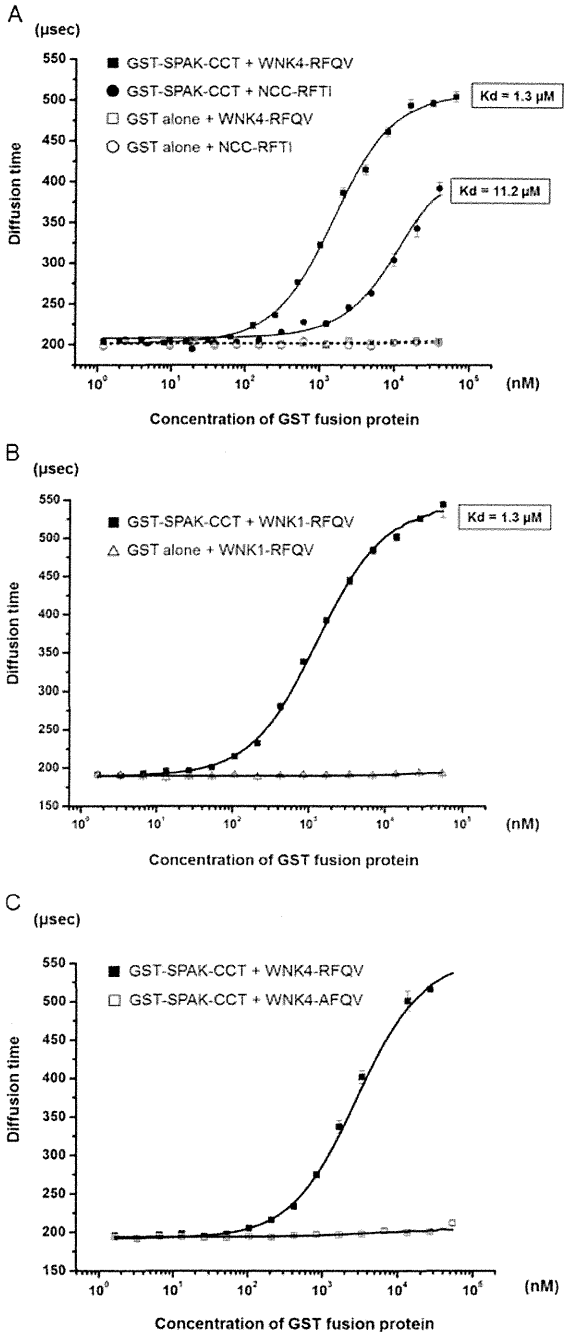

Figure 1 The binding of SPAK with WNK and NCC was detected by a newly developed FCS-based assay

(**A**) The dissociation curve of SPAK with WNK4 and NCC. Fluorescent TAMRA-labelled small peptides that contain the RFQV (Arg-Phe-Gln-Val) motif in WNK4, named WNK4-RFQV (2.7 nM), and the RFTI (Arg-Phe-Thr-Ile) motif in NCC, named NCC-RFTI (2.7 nM), were mixed with the GST-fusion protein of the CCT domain of SPAK (GST–SPAK-CCT) at various concentrations (1–6.5×10^4 nM). Extension of the diffusion time was observed as the concentration of GST–SPAK-CCT increased. (**B**) The dissociation curve of SPAK with WNK1. Fluorescent TAMRA-labelled small peptides that contain the RFQV motif in WNK1, named WNK1-RFQV (2.7 nM), were mixed with GST–SPAK-CCT at various concentrations (1–5.7×10^4 nM). Extension of the diffusion time was observed as the concentration of GST–SPAK-CCT increased. (**C**) The dissociation curve of SPAK with WNK4-AFQV mutant. Fluorescent TAMRA-labelled WNK4 peptide in which the RFXV motif was mutated and which does not bind to SPAK, named WNK4-AFQV, was mixed with GST–SPAK-CCT at various concentrations (1–5.7×10^4 nM). WNK4-AFQV hardly affected the diffusion time.

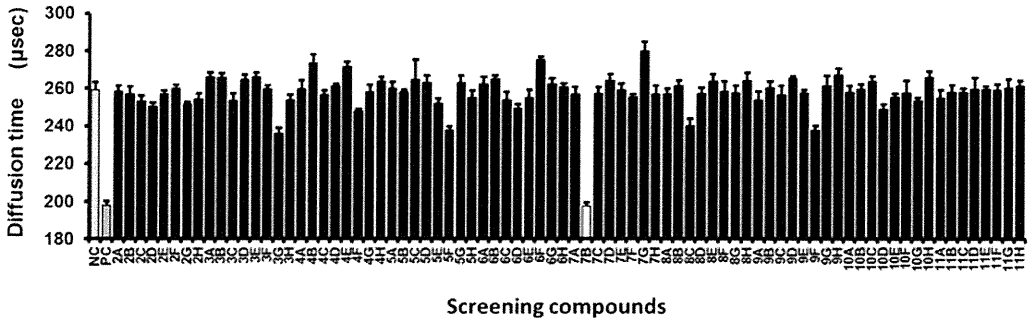

Figure 2 High-throughput screening of WNK–SPAK-binding inhibitors

Compounds in a chemical library were added to the mixed solution of WNK4-RFQV and GST–SPAK-CCT. WNK4-RFQV plus GST–SPAK-CCT without any compounds was used as the negative control (NC, solvent control as a binding state), and WNK4-AFQV (non-binding peptide) plus GST–SPAK-CCT was used as the positive control (PC, dissociation control). White bars show the inhibition of binding by the compounds ($n = 5$, means ± S.E.M.).

measurements were repeated five times per sample. K_d and IC_{50} values were calculated by Origin 8.1 data analysis and graphing software (OriginLab).

Biacore analysis

Binding was analysed in a Biacore T100 system. GST–SPAK-CCT was bound to a CM5 sensor chip (pH 4.0, 19000 response units). The indicated concentrations of compounds in Tris-based buffer (50 mM Tris/HCl, pH 7.5, 150 mM NaCl, 10 mM $MgCl_2$ and 0.05 % Tween 20) were injected over the immobilized GST–SPAK-CCT for 40 s at a flow rate of 60 μl/min. Interactions between each compound and GST–SPAK-CCT were analysed, and steady-state binding was determined at each concentration. Dissociation of compounds was monitored over 120 s.

Statistical analysis

Statistical significance was evaluated using an unpaired t test. P values <0.05 were considered statistically significant. When more than three groups were compared, one-way ANOVA was used, followed by Fisher's post-hoc test. Data are presented as means ± S.E.M.

RESULTS

Detection of the binding of SPAK to WNK and NCC by FCS

The CCT domain in OSR1/SPAK forms a protein fold that interacts with the Arg-Phe-Xaa-Val/Ile (RFxV/I) motif through a surface-exposed groove. Mutation of each residue within this motif in WNKs abolishes binding to SPAK/OSR1 [22]. The CCT domain functions as a multipurpose docking site, enabling SPAK/OSR1 to interact with substrates (NCC/NKCC1/NKCC2) and activators (WNK1/WNK3/WNK4) [28–30]. To identify chemical compounds that disrupt this binding, we established a system capable of high-throughput screening to detect the binding of two molecules. FCS is a method capable of measuring the fluctuation rate of a fluorescently labelled single peptide as output of the translational diffusion times. When a fluorescently labelled molecule binds to another molecule, the translational diffusion time is extended by increasing the apparent molecular mass [27]. In accordance with this principle, we first tested whether we could detect the binding of SPAK to WNK and NCC.

Fluorescent TAMRA-labelled small peptides containing the RFQV (Arg-Phe-Gln-Val) motif in WNK4 were mixed with the GST-fusion proteins of the CCT domain of SPAK (GST–SPAK-CCT) at various concentrations (2–6.5×10^4 nM) in the wells of 384-well microtiter plates. The translational diffusion time in each well was measured by FluoroPoint-Light (Olympus). The addition of GST–SPAK-CCT dose-dependently increased the translational diffusion time of WNK4-RFQV, indicating that this method could detect binding. The dissociation curve between WNK4 and GST–SPAK-CCT obtained in the FCS assay is shown in Figure 1(A) (apparent K_d of 1.3 μM). Furthermore, to investigate whether WNK1 could also interact with SPAK, we prepared a fluorescent TAMRA-labelled WNK1 peptide (WNK1-RFQV), which shares 59 % amino acid identity with WNK4-RFQV (shown in Supplementary Figure S1 at http://www.biochemj.org/bj/455/bj4550339add.htm). We analysed the interaction of WNK1-RFQV and GST–SPAK-CCT by using FCS, and the results are shown in Figure 1(B). WNK1-RFQV exhibited almost the same behaviour as WNK4-RFQV (apparent K_d of 1.3 μM), indicating that WNK1 interacts with SPAK via the CCT domain similarly to WNK4. In addition, the binding of GST–SPAK-CCT to an RFxV/I motif in NCC, which is the substrate of OSR1/SPAK, was also confirmed in this assay (Figure 1A, apparent K_d of 11.2 μM). The affinity of GST–SPAK-CCT for NCC was 10-fold lower than the affinity for WNK4 and WNK1.

Screening of chemical compounds that disrupt the binding of GST–SPAK-CCT to WNK4

We used this newly developed system to screen 17000 compounds owned by the Tokyo Medical and Dental University Chemical Biology Screening Center. Since the compounds were dissolved in 1 % DMSO, we first checked whether the FCS assay was affected by DMSO. We confirmed that DMSO at various concentrations from 0.2 % to 10 % (the final concentration used for screening was 1 %) did not affect the diffusion time of either peptide (results not shown). As a positive control indicating the inhibition of interaction between WNK4 peptide and GST–SPAK-CCT, we prepared TAMRA-labelled WNK4 peptide in which the RFXV motif was mutated to AFQV (named WNK4-AFQV), which reportedly did not bind to GST–SPAK-CCT [22]. As expected, WNK4-AFQV did not affect the diffusion time (Figure 1C), indicating that it behaved as a positive control of binding inhibition.

Representative results of the initial screening are shown in Figure 2. Although most of the compounds showed no inhibitory effects, a few compounds restored the diffusion time increased by the binding to GST–SPAK-CCT. We judged that the compound had an inhibitory effect on the binding when the measured

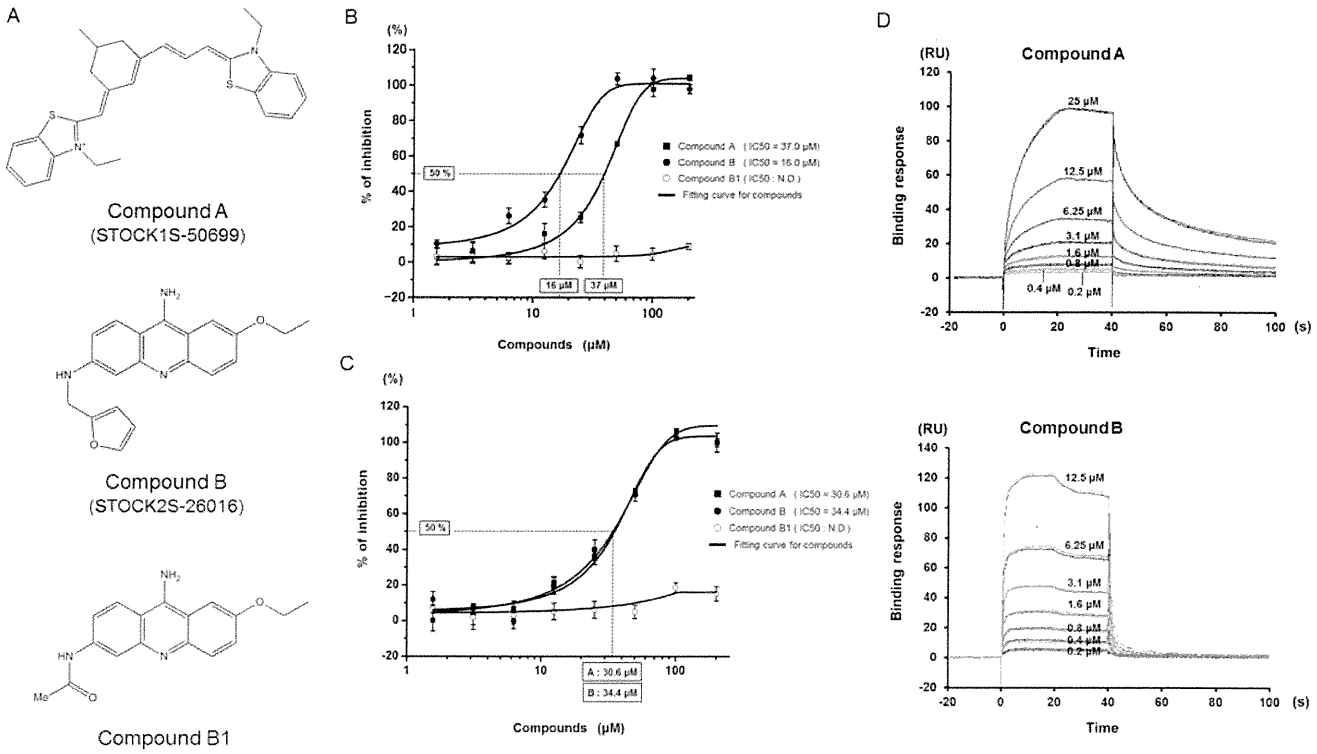

Figure 3 Two promising compounds of WNK–SPAK-binding inhibitors obtained by FCS screening

(**A**) Chemical structures and substance names of two promising inhibitors. Compound B1 is a close homologue of compound B that has no inhibitory activity. (**B**) Confirmation of binding inhibition of WNK4 and SPAK by compounds A and B. The two compounds were added to a mixed solution of TAMRA-WNK4 (RFQV) and GST–SPAK-CCT at various concentrations (1.5–200 μM). The IC_{50} values of compound A and B were 37 μM and 16 μM respectively. Compound B1 showed no inhibitory effect. (**C**) Confirmation of binding inhibition of WNK1 and SPAK by the compounds. Results similar to (**B**) were obtained. The IC_{50} values of compound A and B were 30.6 μM and 34.4 μM respectively. Compound B1 showed no inhibitory effect. (**D**) Binding of the two compounds to the CCT domain of SPAK (GST–SPAK-CCT) determined by Biacore™ assay. Sensorgram shows concentration-dependent binding of two compounds to GST–SPAK-CCT. GST–SPAK-CCT was ligated on to a CM5 sensor chip by standard primary amine coupling chemistry. Compounds were injected for 40 s over the immobilized GST–SPAK-CCT at a flow rate of 60 μl/min. The K_d values (steady state) of compounds A and B were 32 μM and 20 μM respectively. N.D., not determined; RU, response units.

diffusion time was within $\pm$10% of the positive control. As a result of the initial screening of 16902 compounds, we obtained 104 primary hits. Along with the secondary screening, we then checked whether these compounds affected the diffusion time of fluorescent peptide alone to exclude a false-positive effect (Supplementary Figure S2 at http://www.biochemj.org/bj/455/bj4550339add.htm). After checking the false-positive effect and reproducibility (Supplementary Figure S2), 94 compounds were excluded. Finally, ten secondary hits were obtained.

FCS and Biacore™ assays of two promising compounds

Figure 3(A) shows the chemical structure of the two compounds that showed the highest inhibitory activity among the ten secondary hits (compounds A and B) and one close homologue of compound B that has no inhibitory activity (compound B1). The substance names of compounds A and B are STOCK1S-50699 (PubChem-CID 5749625) and STOCK2S-26016 (PubChem-CID 3135086) respectively. Figure 3(B) shows the results of the *in vitro* FCS assay of these drugs for the inhibition of the binding of WNK4 and SPAK. The IC_{50} values of compound A and B were 37 μM and 16 μM respectively. Furthermore, we tested whether the binding of SPAK to WNK1 as well as WNK4 was inhibited by the same compounds. As shown in Figure 3(C), the inhibitory effects of both compounds on WNK1 were similar to those for WNK4. Interestingly, compound B1 (Figure 3A), a structurally close homologue of compound B, did not show an inhibitory effect in the FCS assay (Figures 3B and 3C), suggesting that the inhibitory effect of compound B might not be a non-specific effect on the binding and also provided some implication about the structure–activity relationship of the inhibitor. In the FCS assay, it is difficult to determine whether the compound binds to WNK or SPAK. Thus, to determine the binding partner, we performed further analysis of the interaction between the hit compounds and GST–SPAK-CCT using Biacore™. As shown in Figure 3(D), it was confirmed that both compounds bound to GST–SPAK-CCT, although the binding kinetics were different. Compound A showed relatively slow binding and dissociation compared with compound B, which may be a benefit in terms of drug properties. The K_d values (steady state) of compounds A and B obtained by the Biacore™ assay were 32 μM and 20 μM respectively. These values were comparable with the values obtained by the FCS assay, clearly suggesting that both hit compounds inhibited the binding of WNK and SPAK by binding to the CCT domain of SPAK.

The two compounds showed inhibitory effects on hypotonicity-induced WNK-SPAK signalling in mpkDCT and MOVAS cells

Next, we tested whether these compounds possess *in vivo* inhibitory activity for WNK signalling using mpkDCT cells (Figures 4A and 4C), which endogenously express SPAK and

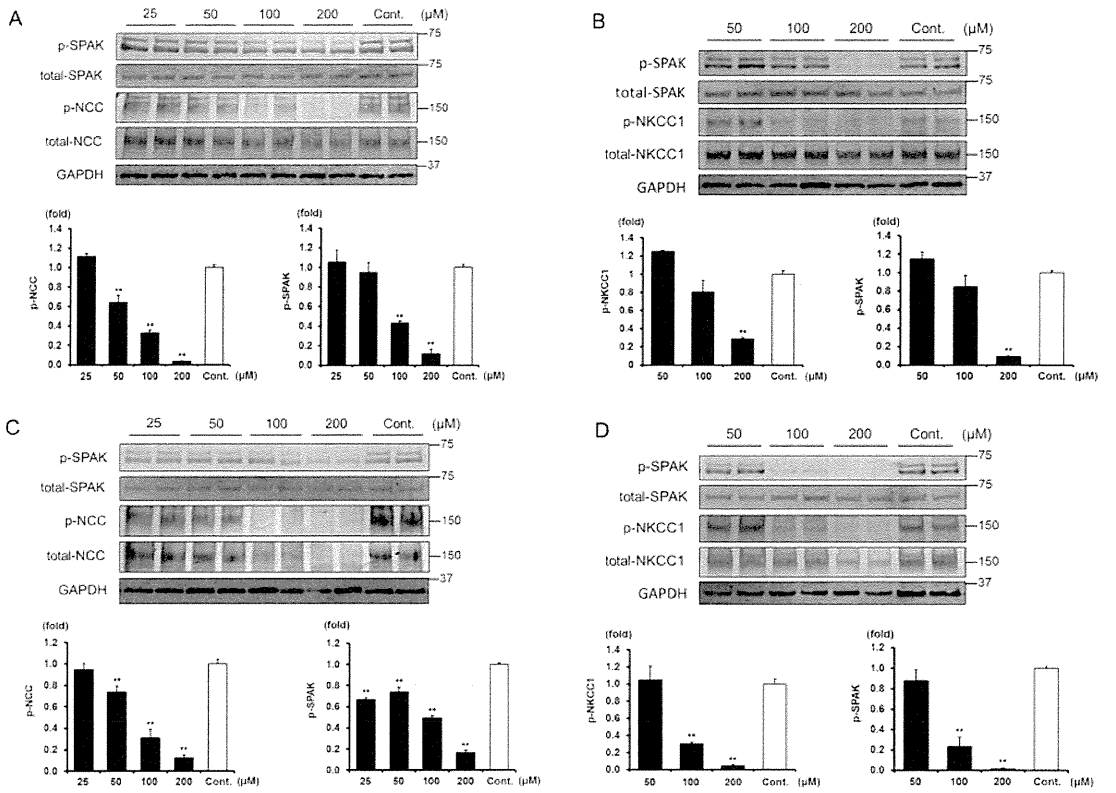

Figure 4 Inhibitory effect of compound A and B on WNK–SPAK signalling in mpkDCT and MOVAS cells

(**A**) The phosphorylation of SPAK and NCC in mpkDCT cells was drastically and dose-dependently reduced by compound A (25–200 μM). The lower panel shows quantification of the results of the blots (**$P < 0.01$, $n = 4$, means ± S.E.M.). (**B**) The phosphorylation of SPAK and NKCC1 in MOVAS cells was drastically and dose-dependently reduced by compound A (50–200 μM). The lower panel shows quantification of the results of the blots (**$P < 0.01$, $n = 4$, means ± SEM). (**C**) Results similar to (**A**) were obtained by treatment with compound B in mpkDCT cells. (**D**) Results similar to (**B**) were obtained by treatment with compound B in MOVAS cells. Cont., control.

NCC [28], and MOVAS cells (Figures 4B and 4D), which endogenously express SPAK and NKCC1 [31]. We used 45 min of hypotonic shock (170 mOsm/g H_2O) to activate WNK signalling. Both compounds A and B dose-dependently inhibited the phosphorylation of endogenous SPAK and NCC in mpkDCT cells and SPAK and NKCC1 in MOVAS cells. To exclude the possibility that the decreases in phosphorylation were due to non-specific effects of the compounds, we evaluated the effect of these compounds on phospho- and total-p38 MAPK (mitogen-activated protein kinase) expression, which is a separate phosphorylation event from WNK-SPAK signalling. As shown in Supplementary Figure S3 (at http://www.biochemj.org/bj/455/bj4550339add.htm), even with the increased concentrations of the compounds, the phosphorylated p38 expression was not reduced, rather slightly increased by these compounds. Compound B1, a non-inhibitory homologue of compound B, also did not affect the phosphorylation of SPAK and NCC (Supplementary Figure S4 at http://www.biochemj.org/bj/455/bj4550339add.htm). These data serve as negative controls to support the specificity of the inhibitory effect of compounds A and B on WNK-SPAK signalling.

DISCUSSION

The current interest in therapeutic antibodies vividly demonstrates the value of a strategy to create drugs by disrupting protein–protein interactions [18]. Therapeutic antibodies have some excellent properties: they are highly specific for their molecular targets, and they tend to be stable in human serum. On the other hand, antibodies are difficult and expensive to manufacture, and they lack oral bioavailability. In addition, antibodies are not cell-permeable; therefore, antagonism of intracellular protein–protein systems has been limited so far. In this respect, if the target proteins are cytoplasmic proteins, the development of small compounds that disrupt protein–protein interactions is highly anticipated.

We have developed a novel screening system for binding inhibitors using FCS. As shown in Figure 1, our FCS method succeeded in detecting the binding between WNK and SPAK. Our FCS system has several advantages. First, immobilization of substrates is not required, unlike the Biacore™ system. Secondly, since the assay is performed in aqueous solution, the binding of molecules occurs under more physiological conditions. Thirdly, our system directly assesses the ability of compounds to disrupt the binding of two molecules. Although Biacore™ can detect the binding of compounds to one of the target molecules with high sensitivity, it does not tell us whether the compounds indeed disrupt the binding of two molecules. Furthermore, our system has a great feature capable of high-throughput screening in 384-well plates.

In this FCS system, in order to detect the binding of two molecules the sensitivity would be better when the apparent molecular mass of a fluorophore changes drastically by binding.

Therefore we used TAMRA-labelled WNK peptides as probes. In this respect, their counterpart, SPAK, should be better in the full-length form than in the partial form (GST–SPAK-CCT). However, the full-length GST–SPAK protein was difficult to obtain in a large amount, mainly due to low solubility and recovery. Thus our binding assay was performed with partial proteins of WNK and SPAK. Therefore we might have missed any compounds that have a greater inhibitory effect on the binding of native full-length proteins. This drawback might be a trade-off for the efficiency of our screening system.

As a result of screening for compounds that disrupt the binding of WNK to SPAK, we obtained two compounds that effectively inhibited the signalling from WNK to NCC and NKCC1 in mpkDCT and MOVAS cells respectively. The amount of total NCC/NKCC1 clearly decreased in the presence of these compounds as the phosphorylation decreased. Similar changes were observed in our previous studies [9,32] and in WNK4-knockout mice [14]. Recently, we showed that the NCC phosphorylation regulated its ubiquitination [33], suggesting that the decrease of NCC/NKCC1 phosphorylation would induce the degradation. In this respect, the changes in phosphorylation would be the primary event. Therefore we only presented phosphorylation of NCC/NKCC1 and SPAK data in the histograms of Figure 4. Nonetheless, it is still possible that our compounds might also block the binding of SPAK to NCC/NKCC1, and the complex formation of SPAK and NCC/NKCC1 might somehow be involved in the stability of the transporters. Further investigation may be necessary on this issue.

The results of the present study clearly demonstrate that the binding between WNK and SPAK is indispensable for WNK signalling *in vivo* and that these compounds are the promising seeds of a new class of anti-hypertensive drugs with dual actions of diuresis and vasodilation. In addition to the antihypertensive property of a WNK-SPAK signalling inhibitor, the recent advancement of WNK research has revealed the possibility of additional therapeutic targets of WNK-SPAK inhibition. WNK3 stimulated glioma invasion by regulating cell volume through NKCC1 activation [34,35]. The knockout of SPAK attenuated intestinal inflammation in mice [36,37]. Those studies suggest the possibility of WNK-SPAK signalling inhibitors that are not just anti-hypertensive drugs. Chemical modification of these compounds would give us better compounds that can be used *in vivo*.

In conclusion, we developed a new high-throughput screening system to identify compounds that disrupt the binding of two molecules. By using this method, we found promising seeds of WNK signalling inhibitors.

AUTHOR CONTRIBUTION

Takayasu Mori established the screening system using FCS and performed the chemical library screening, Biacore™ assay and cell culture studies, and wrote the paper. Yuko Watanabe, Mari Ishigami-Yuasa, Shinya Fujii and Hiroyuki Kagechika prepared the compounds in the chemical library. Eriko Kikuchi, Eisei Sohara, Tatemitsu Rai and Sei Sasaki helped Takayasu Mori in general experimental procedures and contributed to data discussion. Shinichi Uchida designed and directed the project and wrote the paper.

FUNDING

This study was supported in part by Grants-in-Aid for Scientific Research (S) from the Japan Society for the Promotion of Science, a Health Labor Science Research Grant from the Ministry of Health Labor and Welfare, the Salt Science Research Foundation [grant number 1026, 1228), a Banyu Foundation Research grant and the Takeda Science Foundation.

REFERENCES

1 Gordon, R. D. (1986) Syndrome of hypertension and hyperkalemia with normal glomerular filtration rate. Hypertension **8**, 93–102
2 Wilson, F. H., Disse-Nicodème, S., Choate, K. A., Ishikawa, K., Nelson-Williams, C., Desitter, I., Gunel, M., Milford, D. V., Lipkin, G. W., Achard, J. M. et al. (2001) Human hypertension caused by mutations in WNK kinases. Science **293**, 1107–1112
3 Kahle, K. T., Rinehart, J., Giebisch, G., Gamba, G., Hebert, S. C. and Lifton, R. P. (2008) A novel protein kinase signaling pathway essential for blood pressure regulation in humans. Trends Endocrinol. Metab. **19**, 91–95
4 McCormick, J. A., Yang, C. L. and Ellison, D. H. (2008) WNK kinases and renal sodium transport in health and disease: an integrated view. Hypertension **51**, 588–596
5 Richardson, C. and Alessi, D. R. (2008) The regulation of salt transport and blood pressure by the WNK-SPAK/OSR1 signalling pathway. J. Cell Sci. **121**, 3293–3304
6 Uchida, S. (2010) Pathophysiological roles of WNK kinases in the kidney. Pflugers Arch. **460**, 695–702
7 Yang, S. S., Morimoto, T., Rai, T., Chiga, M., Sohara, E., Ohno, M., Uchida, K., Lin, S. H., Moriguchi, T., Shibuya, H. et al. (2007) Molecular pathogenesis of pseudohypoaldosteronism type II: generation and analysis of a Wnk4(D561A/+) knockin mouse model. Cell Metab. **5**, 331–344
8 Moriguchi, T., Urushiyama, S., Hisamoto, N., Iemura, S., Uchida, S., Natsume, T., Matsumoto, K. and Shibuya, H. (2005) WNK1 regulates phosphorylation of cation-chloride-coupled cotransporters via the STE20-related kinases, SPAK and OSR1. J. Biol. Chem. **280**, 42685–42693
9 Chiga, M., Rai, T., Yang, S. S., Ohta, A., Takizawa, T., Sasaki, S. and Uchida, S. (2008) Dietary salt regulates the phosphorylation of OSR1/SPAK kinases and the sodium chloride cotransporter through aldosterone. Kidney Int. **74**, 1403–1409
10 Garg, P., Martin, C. F., Elms, S. C., Gordon, F. J., Wall, S. M., Garland, C. J., Sutliff, R. L. and O'Neill, W. C. (2007) Effect of the Na-K-2Cl cotransporter NKCC1 on systemic blood pressure and smooth muscle tone. Am. J. Physiol. Heart Circ. Physiol. **292**, H2100–H2105
11 Akar, F., Jiang, G., Paul, R. J. and O'Neill, W. C. (2001) Contractile regulation of the Na^+-K^+-$2Cl^-$ cotransporter in vascular smooth muscle. Am. J. Physiol. Cell Physiol. **281**, C579–C584
12 Meyer, J. W., Flagella, M., Sutliff, R. L., Lorenz, J. N., Nieman, M. L., Weber, C. S., Paul, R. J. and Shull, G. E. (2002) Decreased blood pressure and vascular smooth muscle tone in mice lacking basolateral Na^+-K^+-$2Cl^-$ cotransporter. Am. J. Physiol. Heart Circ. Physiol. **283**, H1846–H1855
13 Talati, G., Ohta, A., Rai, T., Sohara, E., Naito, S., Vandewalle, A., Sasaki, S. and Uchida, S. (2010) Effect of angiotensin II on the WNK-OSR1/SPAK-NCC phosphorylation cascade in cultured mpkDCT cells and *in vivo* mouse kidney. Biochem. Biophys. Res. Commun. **393**, 844–848
14 Castañeda-Bueno, M., Cervantes-Pérez, L. G., Vázquez, N., Uribe, N., Kantesaria, S., Morla, L., Bobadilla, N. A., Doucet, A., Alessi, D. R. and Gamba, G. (2012) Activation of the renal Na^+:Cl^- cotransporter by angiotensin II is a WNK4-dependent process. Proc. Natl. Acad. Sci. U.S.A. **109**, 7929–7934
15 Sohara, E., Rai, T., Yang, S. S., Ohta, A., Naito, S., Chiga, M., Nomura, N., Lin, S. H., Vandewalle, A., Ohta, E. et al. (2011) Acute insulin stimulation induces phosphorylation of the Na-Cl cotransporter in cultured distal mpkDCT cells and mouse kidney. PLoS ONE **6**, e24277
16 Nishida, H., Sohara, E., Nomura, N., Chiga, M., Alessi, D. R., Rai, T., Sasaki, S. and Uchida, S. (2012) Phosphatidylinositol 3-kinase/Akt signaling pathway activates the WNK-OSR1/SPAK-NCC phosphorylation cascade in hyperinsulinemic db/db mice. Hypertension **60**, 981–990
17 Chen, J., Gu, D., Huang, J., Rao, D. C., Jaquish, C. E., Hixson, J. E., Chen, C. S., Lu, F., Hu, D., Rice, T. et al. (2009) Metabolic syndrome and salt sensitivity of blood pressure in non-diabetic people in China: a dietary intervention study. Lancet **373**, 829–835
18 Arkin, M. R. and Wells, J. A. (2004) Small-molecule inhibitors of protein-protein interactions: progressing towards the dream. Nat. Rev. Drug Discov. **3**, 301–317
19 Hu, L., Magesh, S., Chen, L., Wang, L., Lewis, T. A., Chen, Y., Khodier, C., Inoyama, D., Beamer, L. J., Emge, T. J. et al. (2013) Discovery of a small-molecule inhibitor and cellular probe of Keap1-Nrf2 protein-protein interaction. Bioorg. Med. Chem. Lett. **23**, 3039–3043
20 Clark, R. C., Lee, S. Y., Searcey, M. and Boger, D. L. (2009) The isolation, total synthesis and structure elucidation of chlorofusin, a natural product inhibitor of the p53-mDM2 protein-protein interaction. Nat. Prod. Rep. **26**, 465–477
21 Berg, T. (2008) Small-molecule inhibitors of protein-protein interactions. Curr. Opin. Drug Discov. Devel. **11**, 666–674
22 Vitari, A. C., Thastrup, J., Rafiqi, F. H., Deak, M., Morrice, N. A., Karlsson, H. K. and Alessi, D. R. (2006) Functional interactions of the SPAK/OSR1 kinases with their upstream activator WNK1 and downstream substrate NKCC1. Biochem. J. **397**, 223–231